Eur. Radiol. 10, 12–35 (2000)

European
Radiology

Review article

Coronary arteries

P. A. Wielopolski[1], **R. J. M. van Geuns**[2], **P. J. de Feyter**[2], **M. Oudkerk**[1]

[1] Department of Radiology, Daniel den Hoed Cancer Center, University Hospital Rotterdam, Groene Hilledijk 301, NL-3075EA Rotterdam, The Netherlands
[2] Thoraxcentre, University Hospital Rotterdam, Dr. Molewaterplein 40, NL-3015GO Rotterdam, The Netherlands

Abstract. Coronary angiography (CA) is presently considered the gold standard for the assessment of the coronary arteries. However, the presence of ionizing radiation, its invasiveness and the small associated risk of morbidity prompted long ago the development of more patient-friendly imaging modalities. A promising technique, magnetic resonance imaging (MRI), has been regarded as the major modality in the coming decade. Although still in its infancy qualitatively, its flexibility and non-invasiveness opens the door for a comprehensive evaluation of the heart and the coronary arteries in one single sitting with high anatomical definition and excellent soft tissue contrast capabilities, double-oblique tomographic sections and the possibility to quantify an innumerable number of cardiovascular physiological parameters. Numerous ideas have been assessed, comprising breath-hold and free-breathing two-dimensional and three-dimensional measurements. New ongoing trials with intravascular contrast agents may provide for all these techniques the long-awaited essential boost for reliable magnetic resonance coronary angiography (MRCA). Introduction of parallel MRI acquisition techniques, such as simultaneous acquisition of spatial harmonics (SMASH) and sensitivity encoding (SENSE) may provide the speed enhancement required to shorten imaging time for all techniques explored to date.

Key words: Magnetic resonance coronary angiography – Two-dimensional – Three-dimensional – Breath-hold – Free breathing – Navigator – Parallel MR imaging

Correspondence to: P. A. Wielopolski

Categorical Course ECR 2000

Introduction

Despite its indisputable standard of reference for the detection of coronary artery stenosis, conventional coronary angiography (CA) is expensive, requires ionizing radiation and its invasiveness poses risks of major complications that can lead to stroke and death. In response, several imaging methodologies have been investigated to help assess, directly or indirectly, the state of the coronary circulation and determine the severity of a coronary lesion with lesser risks while providing a less costly and safer alternative to patient screening and follow-up.

Localizing coronary lesions and their possible impact is key to how disease management can carry through in a given cardiac patient. Although several non-invasive imaging modalities have been available clinically that can provide this information, MRI deserves special attention. Magnetic resonance imaging is devoid of harmful radiation exposure ensuring study repeatability and it can deliver high-resolution images with superb contrast characteristics in any desired orientation, especially suitable to study the coronary anatomy. The technique can also furnish functional parameters to complement the evaluation of a detected coronary lesion (e. g., through myocardial motion analysis and perfusion mapping during rest and stress tests). With clear advantages over other techniques, MRI could broaden enormously the scope in the assessment of cardiovascular diseases in preventive medicine if reliable patient screening could be performed before symptoms of coronary artery disease appear that would require immediate catheterization.

In this review we put in perspective and generalize on all magnetic resonance coronary angiographic (MRCA) techniques that have been investigated to date. To accomplish this, an outlook on basic scanning concepts and possibilities already explored for MRCA is presented. We generalize on the potential impact of hardware and software advances on newer "dedicated cardiovascular" MRI units on current MRCA concepts, the commercial appearance of intravascular contrast agents

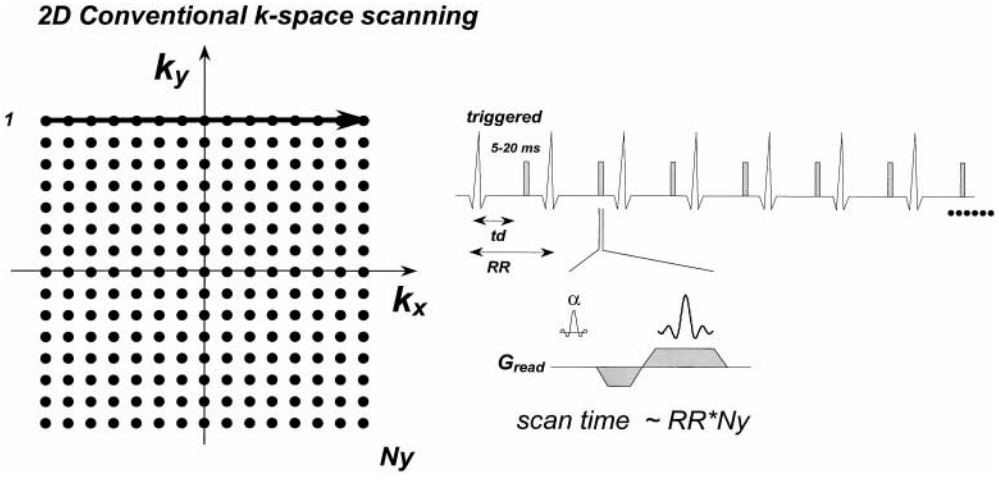

Fig. 1. Conventional 2D k-space encoding. One single line of k-space is acquired per heartbeat (shown for a GRE readont). Imaging time equals the number of in-plane phase-encoding lines selected. Temporal resolution is excellent, with each readout accomplished in several milliseconds. In the example, 15 heartbeats are needed to cover the entire k-space matrix. k_x frequency encoding; k_y phase encoding; N_y number of in-plane phase-encoding steps; *td* delay to acquisition; *RR* cardiac period; G_{read} readout gradient waveform

and novel acquisition strategies that all together may reduce dramatically the imaging time for "the integrated assessment" of the heart and coronary arteries in the near future.

Challenges to tomographic imaging: the success of conventional coronary angiography

Native coronary arteries not only have a small caliber, ranging between 2 and 5 mm, but their path over the heart is generally tortuous and they are subjected to the pumping action of the heart and respiration. The coronary vessels mostly curve around the wall of the cardiac ventricles, making it difficult to find a single tomographic imaging plane that can encase entirely a coronary branch.

The success of CA for the assessment of the coronary arteries is based on simple facts. Conventional CA is photographic in nature, enjoying exquisite temporal resolution with a frame rate reaching 60 frames per second and high in-plane spatial resolution, of the order of 0.1×0.1 mm^2 for current digital imaging systems. But most adequate to CA is the use of selective contrast injections, targeting directly left and right coronary artery trees. Therefore, CA can render projection images of the entire coronary path over the heart without the interference of cardiac chambers and myocardium. Additionally, the fluoroscopic nature of CA provides information on the dynamics of the contrast media injected, giving an intuitive indication to the coronary artery flow patterns during cine review. This can be considered a real asset for CA, still to be seen applied to tomographic imaging techniques.

The aforementioned characteristics of CA impose large constraints on any non-invasive tomographic technique; therefore, no other imaging modality can fully integrate all the versatility provided by CA, lacking spatial resolution, acquisition speed, or coverage. Magnetic resonance imaging is no exception to the rule, temporal and spatial resolution being mutually exclusive parameters. In addition, with non-invasiveness the current strength of MRI, selective injection of contrast agents is not a viable option for selective MRCA, making projection imaging, in essence, not possible unless tagging techniques with subtraction are used. Since MRI can be regarded relatively slowly when high-resolution images are attempted (image resolution is difficult to attain in a single-shot technique with temporal resolution < 60 ms), a composite raw data set must be formed over several heart cycles, making it susceptible to cardiac motion and arrythmias. Another consideration that must be present is that image resolution is also susceptible to respiratory motion.

MR imaging techniques: spin echoes and gradient-recalled echoes

Two different techniques can be applied to view the coronary arteries. Spin echo (SE) scans and variants (turbo-SE, fast-SE) can produce excellent anatomical images of the heart and great vessels with images in which signal suppression in blood-filled compartments is typical in providing improved contrast. Spin-echo-based techniques are regarded as "black-blood" techniques and are ideal to observe the vessel lumen and, eventually, vessel walls if the signal-to-noise ratio (SNR) and resolution is sufficient. On the contrary, gradient-recalled echo (GRE)-based techniques provide, in general, the opposite contrast by making use of the signal enhancement possible from inflow of non-saturated blood to the region of interest to produce "bright-blood" images. Additionally, GRE techniques are amenable to both two-dimensional (2D) and three-dimensional (3D) imaging formats.

Technique evolution: from slow to ultrafast

To eliminate cardiac motion interference in image resolution (blurring and ghosting removal) it is necessary to synchronize the image acquisition to a specific phase of the cardiac cycle. This is achieved by triggering the acquisition to the acquired ECG signal by a physiological monitoring unit. Both ECG-triggered SE and GRE techniques as conceived over a decade ago are extreme-

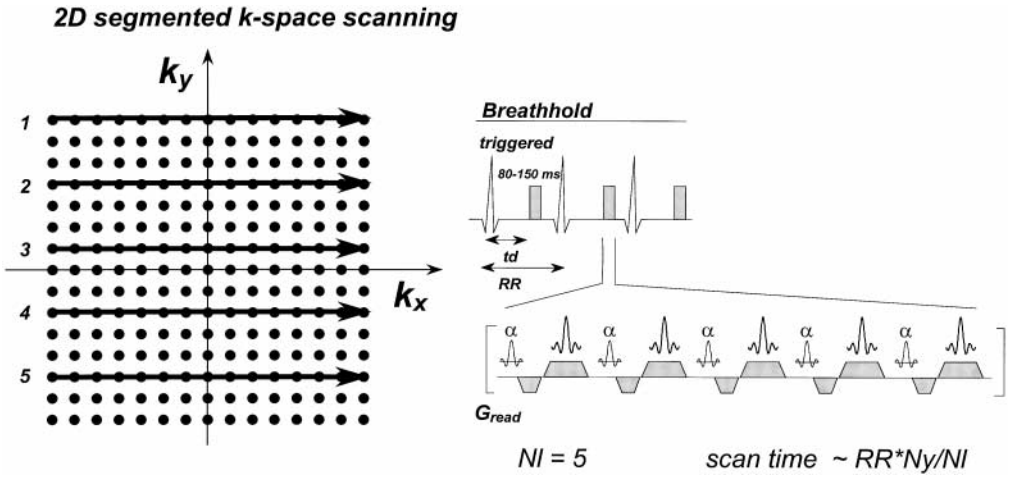

Fig. 2. Segmented 2D k-space encoding. Taking advantage of the period the heart remains quiet during mid-late diastole, the acquisition window can be increased to encase several lines of k-space in an interleaved fashion (shown for a GRE readont). Time resolution is usually of the order of 50–150 ms depending on heart rate. Imaging time in heartbeats is equal to the number of phase-encoding lines divided by the number of lines collected per heartbeat. In the example, the entire k-space data is collected in three heartbeats. k_x frequency encoding; k_y phase encoding; *NI* number of lines scanned in acquisition window; N_y number of in-plane phase-encoding steps; *td* delay to acquisition; *RR* cardiac period; G_{read} readout gradient waveform

ly slow for cardiac imaging. A single line of data was acquired per cardiac phase and required as many heartbeats as in-plane phase-encoding lines to achieve a desired resolution (assuming a 2D scan with a single average; see Fig. 1). Because repetition times (TR) could be shortened to several milliseconds with GRE techniques, such as with turbo FLASH scanning [1, 2, 3], heart motion could be frozen by scanning all in-plane phase encodes in less than 300 ms after detecting the ECG signal with crude spatial resolution (e. g., TR = 3 ms, 64 × 128 matrix, 6.4 × 3.2-mm^2 in-plane resolution). A compromise between spatial and temporal resolution was offered soon enough with 2D segmented GRE [4, 5], a multi-shot modification collecting a reduced set of lines over multiple cardiac periods (Fig. 2). For MRCA, advantage was taken that imaging could be performed during a small interval in mid-late diastole, a moment during which the heart could be considered fairly stationary (60–150 ms, depending on heart rate and coronary segment of interest) [6]. A similar technique, multi-shot spiral imaging, was also conceived that reduced possible signal loss and flow misregistration from fast-moving blood in the coronary arteries (Fig. 3) [7]. Fast-SE techniques, the SE equivalent to the segmented GRE concept, have also found widespread applications in the thorax for assessing cardiac and coronary anatomy within comfortable breath-holds [8], or with free-breathing techniques to augment patient comfort [9]. As mentioned previously, fast-SE variants have been targeted towards black-blood contrast, opposite to the bright blood appearance on GRE scans.

With improved gradient imaging hardware in newer MRI units (especially those called "dedicated cardiac" MR scanners), stronger and faster imaging gradients can be used advantageously to speed up data acquisition, e.g to obtain better coverage with 3D scans by packing more data into that mid-late diastolic period with the heart standstill. Since gradient power has increased by more than 50 times within a decade (direct comparison of gradient-strength rise times), we can envision two distinctive ways to use this power to our advantage (Fig. 4). In one case, the readout bandwidth can be maintained narrow while the proceeding gradients prior to signal readout can be scaled substantially in strength with reduced application times (compare Fig. 4 a,b). Therefore, a shorter TE can be accomplished under the same SNR conditions, improving flow signal behavior, e. g., with velocity-compensated waveforms (Fig. 5). Because higher readout gradients can be utilized during data acquisition, the readout bandwidth can be increased accordingly in order to sample the echo faster (Fig. 4 c). In this case, TE can be shortened dramatically with reduced sensitivity to flow dephasing and flow displacement. A penalty for using higher readout bandwidths is a reduction in the SNR available. The SNR is proportional to $BW^{-1/2}$, where BW indicates the acquisition bandwidth. An increase in acquisition bandwidth can be compensated by using a 3D scanning protocol. Three-dimensional acquisitions can cancel out the noise increase from broader bandwidth acquisitions by an additional factor of $(\text{partitions})^{1/2}$. Figure 5 illustrates phantom examples of the flow behavior improvement possible with high-performance gradients. These improvements are applicable to any GRE MRCA technique. For fast-SE acquisition schemes improvements are seen generally with shorter interecho spacings at constant readout bandwidth.

The increasing availability of phased-array coil receivers to provide enhanced SNR over wide fields of view (FOV), e. g., panoramic array imaging, offer further reductions in TR and makes it practical to acquire more data lines per unit time with larger readout bandwidths. This SNR boost permits to augment the resolution per unit time and the possibility to acquire breathhold 2D multislice and 3D cardiac examinations with

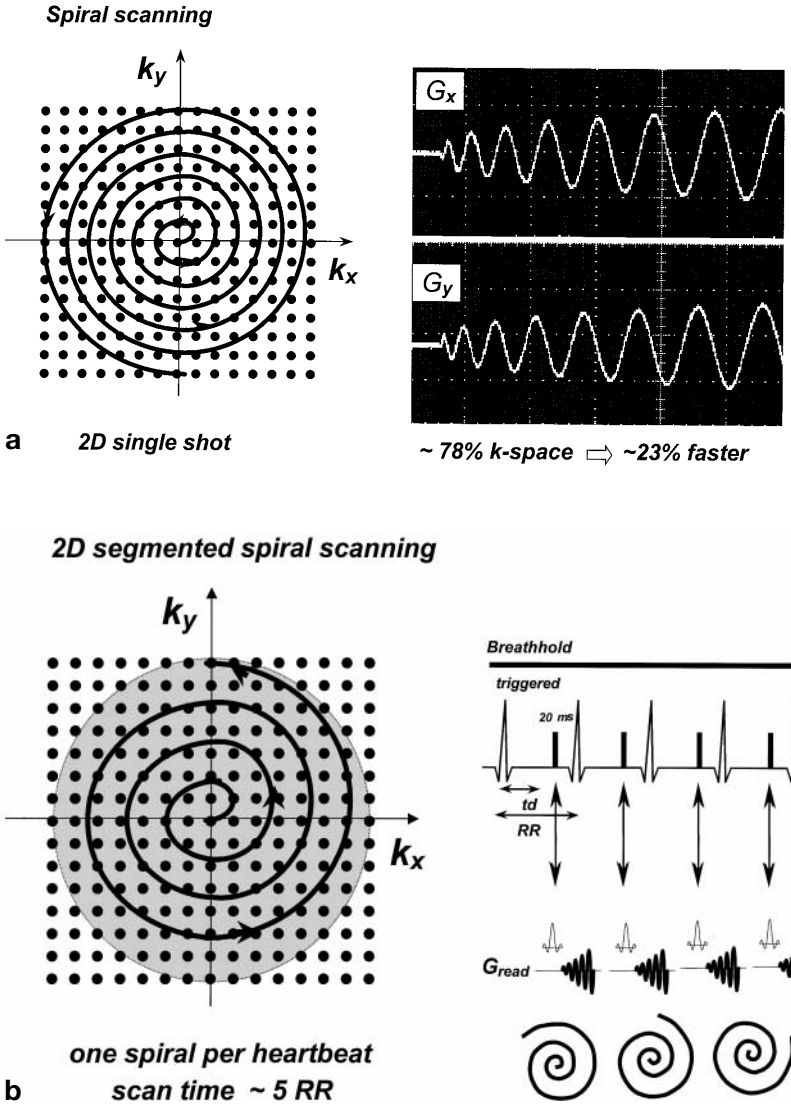

Fig. 3 a, b. Single-shot and segmented 2D spiral k-space encoding. **a** Spiral encoding process. In essence, the in-plane imaging gradients are oscillated in tandem (oscilloscope traces shown) to accomplish a spiral trajectory in k-space. Spiral permits a time savings of 23% over conventional spin-warp scanning. **b** To improve resolution k-space is covered with pieces of spiral trajectories that are rotated accordingly on every heartbeat to provide uniform coverage over k-space. This encoding strategy has very good flow properties but is susceptible to off-resonant effects (producing some blurring) that must be corrected before image presentation through post-processing and needs high-quality gradient hardware to obtain the desired trajectory. k_x frequency encoding; k_y phase-encoding; *td* delay to acquisition; *RR* cardiac period; G_{read} readout gradient waveform

more adequate coverage and spatial and temporal resolution. To fully utilize phased-array coil technology and the strength provided by the newest gradient hardware, 2D and 3D variants of the echo-planar imaging (EPI) technique can be considered for MRCA (Fig. 6) [10]. A suitable combination between GRE and EPI readouts can provide reduced sensitivity to field inhomogeneities (e.g., susceptibility artefacts from sternal wires) and a better compromise between resolution and acquisition speed for 2D MRCA [11].

MRCA techniques

SE-based techniques

The black-blood nature of cardiac-triggered SE techniques and fast-SE variants can demonstrate sections of coronary arteries fairly consistently. Occasionally, the proximal coronary arteries were appreciated in early days when blurring from respiration was not excessive, as illustrated in a study by Paulin et al. using conventional ECG-gated multislice multiphase SE [12]. With the introduction of k-space segmentation with fast-SE scans, studies can be accomplished in a comfortable breath-hold yielding excellent results for black-blood MRCA (Fig. 7). McConnell et al. has further investigated the use of fast-SE scans with respiratory synchronized techniques to produce black-blood images with submillimeter resolution, aiming to improve the quantification of coronary artery stenosis and a first attempt to study the coronary artery wall [9]. With half-Fourier acquired single-shot turbo spin echo (HASTE), a single-shot modification of fast-SE cardiac anatomy has been studied with readout times of 300 ms [13], providing the possibility to obtain rough shots of the coronary arteries and coronary artery bypass grafts (CABG), as demonstrated in Fig. 8. Black-blood consistency in all fast-SE variants that have been used for cardiac studies use a black-blood preparation referred to as PRESTO [14]. This technique is very robust and uses a non-selective inversion rapidly followed by a selective re-inversion. Using the inversion time of blood as inflow delay, blood that has moved into the imaging slice will have

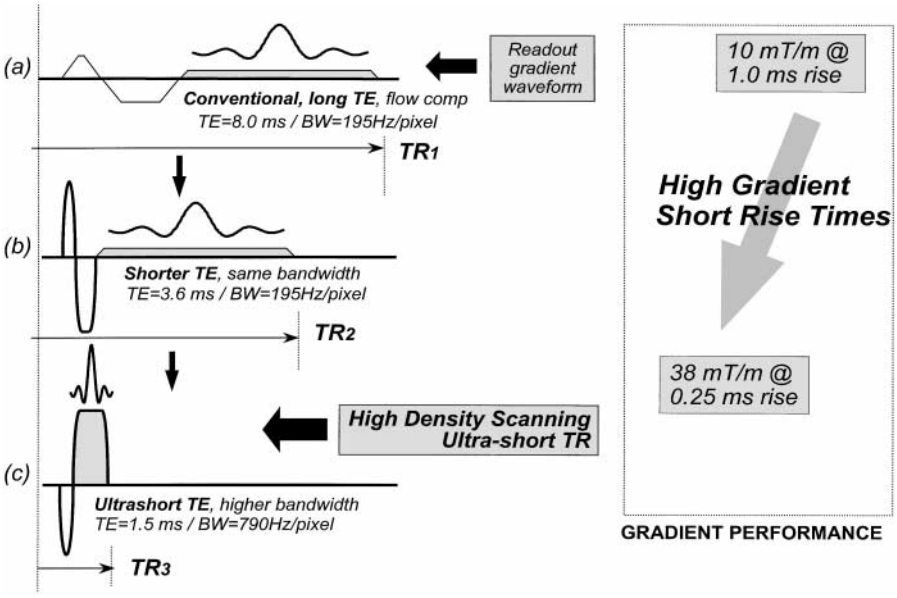

Fig. 4 a–c. Effects of improved gradient hardware on acquisition speed and readout bandwidth. **a** Example velocity compensated GRE waveform along the frequency-encoding direction calculated for an imaging system with a maximum gradient strength of 10 mT/m and a rise time of 1 ms. **b** Similar choice for imaging bandwidth as in **a**, but using stronger and faster imaging gradients permits a shorter TE with a gradient system using 38 mT/m and 0.25-ms rise time. **c** Using full gradient strength and speed, ultrashort TE is possible using high bandwidth acquisition conversely shortening also dramatically the time to acquire the MR signal. The repeat times possible, denoted by TR_1, TR_2, and TR_3, respectively, can vary dramatically ($TR_3 << TR_2 < TR_1$). Only for **c** can TR be made dramatically shorter because readout time is not time-consuming anymore. In general, the RF excitation for **c** takes as long to execute as the readout time, making this solution more suitable for 3D imaging protocols to improve signal-to-noise ratio (SNR) at high bandwidth readouts. Values were computed for a 256 matrix scan at FOV = 200 mm and 64 points prior to the echo (1280 ms RF excitation)

no signal and appear black. Fortunately, this inflow delay mostly coincides with mid-late diastole.

GRE techniques

Gradient-recalled-echo techniques provide greater flexibility for MRCA. Several variants have been explored using 2D and 3D scans combined with breath-hold and free-breathing measurements. It is sensitive to subdivide all MRCA techniques into three technique "generations", with a similar subdivision as suggested recently by Duerinckx (Fig. 9) [15]. The first-generation technique considers scans performed with 2D breath-hold segmented GRE and spiral scanning. For the second-generation four free-breathing strategies have been conceived: averaging multiple acquisitions [16, 17], respiratory gating using respiratory bellows [18], retrospectively respiratory navigator gated acquisition and reconstruction [19, 20], and prospective real-time navigator respiratory data collection [21, 22, 23, 24, 25]. For the third-generation techniques we consider all breath-hold MRCA scans that make use of high-performance gradients to cover either a large heart volume for localization or target with higher resolution a small volume along the coronary arteries [10, 26, 27, 28]. Hybrid approaches using navigator echoes can be incorporated in first- and third-generation techniques to make it possible for data collection over multiple breath-holds using a respiratory feedback monitor (screen or indicator) to warn the patient to reproduce the same breath-hold position [29]. Another approach has also been applied in breath-hold 2D MRCA to correct only the reconstructed image location based on diaphragm position (or heart) to improve inter-slice correlation and aid in the review [30, 31]. The feedback approach can improve SNR in composite data sets [32] and has been attempted for 3D imaging as well [33, 34].

From all combinations possible, 2D breath-hold MRCA scans, 3D retrospective respiratory navigator gated MRCA and a preliminary assessment of prospective respiratory navigator MRCA and breath-hold 3D targeted-volume MRCA have been evaluated clinically (with patient populations ≥ 20; see Table 1). Three-dimensional prospective respiratory navigator MRCA scans are being assessed in a multi-centre trail at this stage (W. Manning, pers. commun.). Other more exotic MRCA techniques further await clinical trials to determine their effectiveness (such as those using EPI methods and composite data collection in several breath-holds using feedback strategies).

Coronary visualization: strategies

Coronary arteries are usually embedded in pericardial fat most of their course. Therefore, current bright-blood GRE MRCA techniques use some form of fat-suppression scheme to separate the signal from coronary artery lumen from surrounding perivascular fat. Proton-density weighting can be used to characterize the signal characteristics of all non-contrast enhanced GRE MRCA

Table 1. Sensitivity and specificity of clinical trials with a patient population ≥ 20 using all three generations of MRCA techniques as compared with conventional angiography (vessels with ≥ 50 % angiographic stenosis). Results are expressed in percent. *n.a.* not available

First-generation MRCA (2D)	No. of subjects	No. of lesions[a]	Sensitivity (%)	Specificity (%)
Manning et al. [38]	39	52	90	92
Manning et al. [40]	72	81	90	n. a.
Duerinckx [41]	20	27	63 (0–75 %)[c]	n. a.
Pennell [42]	39	55	85[d]	n. a.
Post [43]	35	35	63 (A)[b] 40 (B)[c]	89 (A)[c] 97 (B)[c]
Yoshino et al. [44]	36	31	83 (LAD) 100 (RCA)	98 (LAD) 100 (RCA)
Second-generation MRCA (3D) (retrospective navigator approach)				
Post et al. [45]	20	21	38	95
Müller [46]	30	54	83	94
Kessler et al. [97]	73	43	65	n. a.
Sandstede et al. [111]	30	37	81	89
Huber et al. [47]	20	53	73	50
Van Geuns [48]	29	26	50	91
Second-generation MRCA (3D) (prospective navigator approach)				
Lethimonnier [50]	20	17	65	93
Third-generation MRCA (3D)				
Van Geuns et al. [57]	34	31	68	97
Regenfus et al. [61]	30	31	77	94

[a] With significant disease
[b] No. of vessels instead of lesions
[c] Variable sensitivities depending on detection threshold used to interpret images: *A* possible stenosis; *B* certain stenosis
[d] Study interpretation not fully blinded
[e] Using projection images for evaluation

techniques. Coronary segments that run close or within the myocardium that are not surrounded with enough fat cannot be well appreciated and the contrast needs to be enhanced using some form of magnetization preparation (MP) scheme prior to data collection on every heartbeat. Two MP schemes have mainly been devised. The first one considers the application of magnetization transfer (MT) irradiation [17, 26], the second, a T2-weighted preparation [35]. Botnar et al. reported a contrast-to-noise ratio enhancement of 123 % with T2 preparation [36]. The end result from these two MPs is similar; however, T2-weighted preparation can have additional advantages. With T2 preparation better differentiation between arteries and veins is possible by accentuating arterial and venous T2 differences by choosing an optimal TE as demonstrated by Brittain et al. (TE ~ 78 ms for $T2_{arteries}$ = 223 ms and $T2_{veins@20\%O2saturation}$ = 35 ms at 1.5 T, a signal ratio of approximately 6.5)

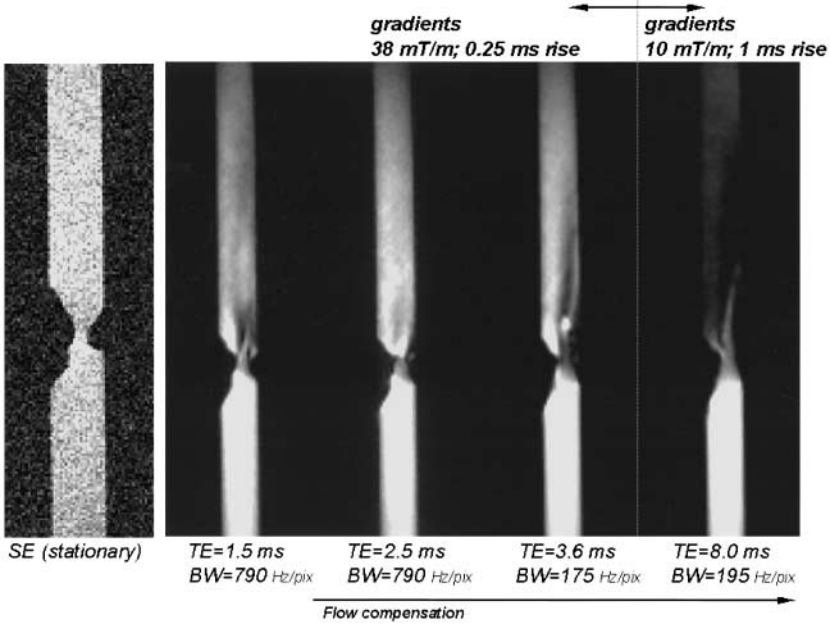

Fig. 5. Behavior of post-stenotic signal loss in a high-grade stenosis phantom with conventional (10 mT/m; 1-ms rise time) and high-performance (38 mT/m; 0.25-ms rise time) flow-compensated GRE sequences as a function of TE and readout bandwidth. The phantom consists of a straight tube with an irregular stenosis characterized by a 70 % stenosis by area. Non-compensated high-performance GRE sequence at TE = 1.5 ms maintains the signal after the stenosis with just a slight attenuation. The best behavior is obtained with a fully flow compensated high-performance GRE sequence at TE = 2.5 ms. The post-stenotic signal loss is extreme with a conventional TE = 8.0 ms when compared with the high-performance equivalent at TE = 3.8 ms with comparable readout bandwidths. The stenosis area is only well depicted for the shortest TEs. The section thickness for all GRE sequence comparisons was 3 mm, and in-plane resolution 0.70 × 0.70 mm^2. Flow direction is from bottom to top with a velocity of 95 cm/s. *SE* 2D spin-echo image, 2 mm, 0.35 × 0.35 mm^2 in-plane resolution; *BW* readout bandwidth in Hz/pixel; *TE* echo time

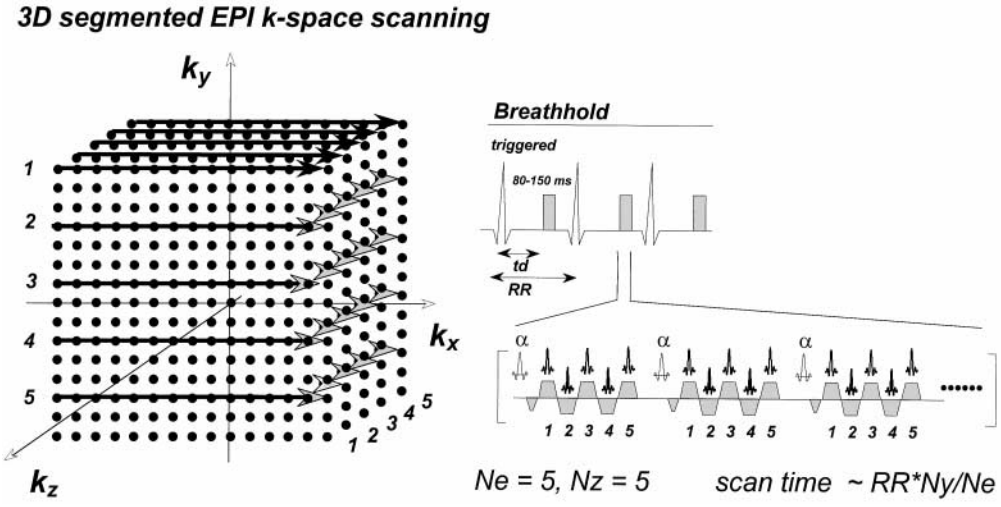

Fig. 6. Segmented 3D echo-planar imaging (EPI) k-space encoding. EPI permits to pack many readouts for each RF excitation (high-density readout) and a large number of lines can be collected within the allotted acquisition window per cardiac period. In this example, three heartbeats fill the entire 3D k-space matrix ($15 \times 15 \times 5$). Comparatively, scan time is the same as for the segmented 2D case depicted in Fig. 2, because it is five times faster, collecting five slice-selection phase-encoding lines per RF excitation. k_x frequency encoding; k_y phase encoding; N_y number of in-plane phase-encoding lines; N_e number of echoes per RF excitation; N_z number of slice-selection phase-encoding steps; *td* delay to acquisition; *RR* cardiac period; G_{read} readout gradient waveform

[37]. In addition, the contrast generated is independent of heart rate (for MT contrast, MT irradiation must otherwise be applied during all the time data is not acquired to make the contrast generation mechanism more heart rate independent). Both MT irradiation and T2-weighted MP decrease the signal from the coronary artery wall providing a more realistic measure of the coronary vessel diameter [36]. Another type of contrast that can be used for coronary artery visualization is that provided by T1-weighted GRE scans. Bright blood can only be achieved if contrast agents are added to the blood pool (extravascular or intravascular) that can shorten the T1 of blood considerably. In this case the T1 shortening should be such that the fat signal is dramatically suppressed for the TR and excitation flip angle considered.

First-generation MRCA: breath-hold 2D techniques

The breath-hold 2D fat-suppressed segmented GRE technique represents the first attempt to resolve the coronary arteries (Figs. 10, 11) [6]. A stack of images oriented parallel to each coronary vessel ensured coverage in case of vessel tortuosity. Scans were performed interactively with breath-hold instructions to the patient and images reviewed in situ (cine display) to appreciate the entire course of a particular coronary vessel. Decisions were made and additional images acquired perpendicular to the vessel path in possible problematic regions (signal inhomogeneities) to better detect vessel narrowing. Perpendicular images take full advantage of inflow effects, helping to obtain higher flow signal and better resolution to visualize any possible narrowing along the way. Manning et al. presented initial encouraging results in 1993 on a young group of adult volunteers [38]. Subsequently, the first clinical study was performed on 39 patients including 74% of the patients with moderate to severe coronary artery stenoses

Fig. 7a–c. Cardiac triggered, breath-hold 2D segmented black-blood fast SE. **a** Orientation along the RCA. **b** Orientation through the aortic root. **c** Orientation along *LM* and *LAD*. Every slice was collected in 22 heartbeats with a time resolution of 105 ms per shot (TE = 57 ms, interecho spacing = 7.12 ms, 15 lines/shot, 5 mm, 240×512 matrix, FOV = 285×380 mm^2). *RCA* right coronary artery; *LM* left main; *LAD* left anterior descending; *Ao* aorta; *RVOT* right ventricular outflow track

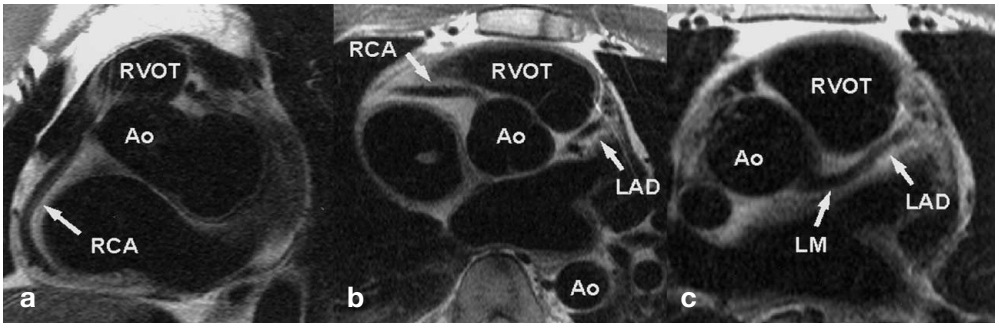

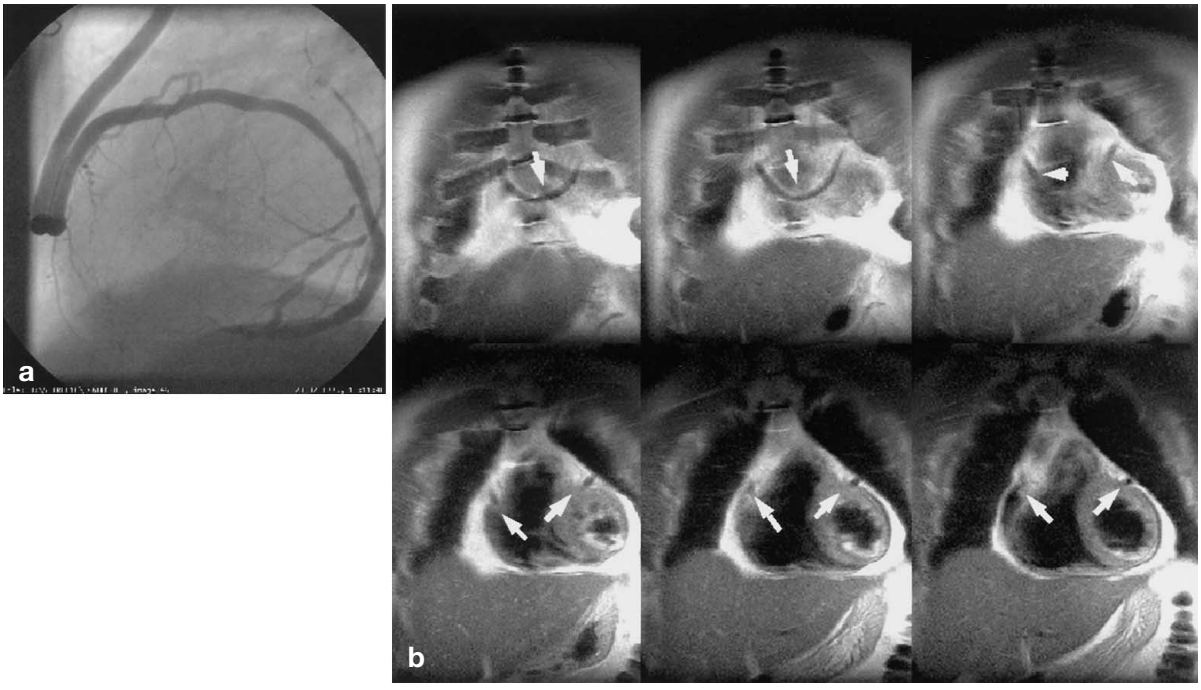

Fig. 8. **a** Cardiac triggered, free-breathing 2D single-shot black-blood fast SE (HASTE) technique for coronary bypass graft localization. **b** Conventional X-ray contrast angiogram of a 50-year-old patient with previous myocardial infarction and presently recurrent angina and with a venous jump graft from the aorta to the left anterior descending, diagonal, intermediate, and marginal branches, and the posterior descending artery. Six sections from 30 collected over 2 min during free-breathing. A single slice of the HASTE technique is acquired every three heartbeats with a time resolution of 395 ms per shot (TE = 30 ms, interecho spacing = 3.8 ms, 5-mm slice thickness, 1-mm overlap, 192 × 256 matrix, FOV = 350 × 350 mm^2). (see also Figs. 21, 22)

(> 50 % diameter stenosis on CA) [39]. In a blinded analysis the overall sensitivity and specificity was 90 and 92 %, respectively. A larger study population showed again similar results [40]; however, trials performed by Duerinckx et al. [41], Pennell et al. [42], Post et al. [43], Yoshino et al. [44] point out the large variability in the results obtained (see Table 1). Breath-hold 2D segmented spiral scans [7] can also be included in this first-generation MRCA group. Clinical results were not reported in parallel and are at an experimental stage and not widely available for clinical use. Segmented 2D spiral scans are becoming popular with dedicated cardiac scanners, producing good-quality data results that rival those obtained with segmented 2D GRE techniques [28].

Second-generation MRCA: improved coverage and SNR with free-breathing 2D and 3D techniques

Multi-slice 2D and 3D GRE MRCA acquisitions have been conceived under multiple scenarios to obtain extended coverage, contiguous slices, and isotropic resolution. The basic idea behind this MRCA generation is to eliminate operator dependence on scan setup, permit image review after the examination is completed, and to produce better SNR MRCA. Given that volume data is collected, post-processing techniques can be applied, such as volume rendering (VR), maximum intensity projection (MIP), or multiplanar reformations (MPR), and show the entire course of a particular coronary segment or a display of the entire coronary tree over the heart. The 3D nature of the data sets can eliminate the overlap of unwanted structures by tissue segmentation during interpretation.

To facilitate patient comfort several free-breathing schemes were evaluated. These comprise (a) averaging multiple acquisitions [16, 17], (b) prospectively respiratory synchronized data collection [18], and (c) retrospectively ordered respiratory gated data [19, 20], the latter two using navigator echoes (signal from a pen-like excitation) to either monitor or correct the displacement of the liver diaphragm or the heart itself during the acquisition.

The method of averaging multiple acquisitions without respiratory synchronization count among the first 3D MRCA techniques used, employed by Paschal et al. [16] and Li et al. [17] with the idea to enhance the SNR of body coil acquisitions while pseudogating the data collection to overcome respiratory ghosting. Because averaging does not provide images at a particular diaphragm position, significant blurring was reported. To decouple and reduce maximally respiratory motion effects on the acquisition Hofman et al. [19] appended the diaphragmatic position provided by a navigator echo to the acquired data (Fig. 12). The navigator echo has been produced using either a spin-echo pen-like excitation generated over the dome of the diaphragm using the intersection of a slice excited by a 90° RF pulse (sagittal) and another slice using a 180° RF pulse (sagittal to coronal orientation) or a single 2D RF excitation

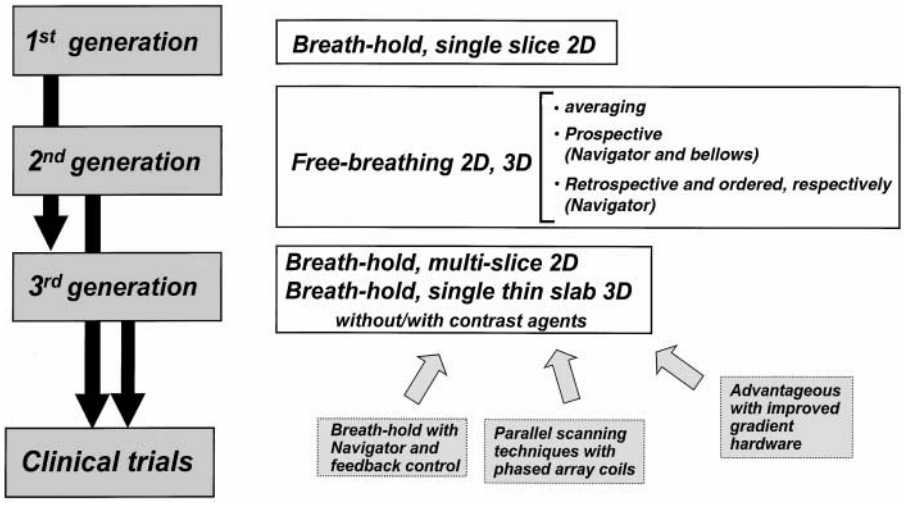

Fig. 9. Three "bright-blood" magnetic resonance coronary angiography (MRCA) technique generations are identified. First-generation MRCA techniques comprise experiments and clinical trial results using the single-slice 2D segmented GRE and spiral scans. Second-generation identifies those MRCA techniques, generally 3D scans, that collect data during free breathing. Third-generation MRCA techniques exclusively aim for volume scans acquired within one or several breath-holds, preferably using high-performance gradient systems and contrast agents. Hybrid setups may be applicable to breath-hold MRCA techniques by using some form of feedback control with navigator echoes to ensure the same diaphragm position for each breath-hold data collection (composite data sets/interslice registration). Clinical trials are still on their way for second- and third-generation techniques

(defining a cylinder). Analysis of the navigator data (position histogram) was then performed to sort the data retrospectively within a predetermined reconstruction gating window (e. g., ± 1, ± 3, or ± 5 mm) that reflected a similar diaphragm position for the entire composite data set (Fig. 13 a). In general, the reconstructed data sets reflect an end-expiration scan in subjects with typical respiratory patterns. To ensure data sampling over the entire respiratory cycle multiple acquisitions were performed for each portion of k-space scanned per heartbeat (a constant oversampling factor of 5 or 6). Scan time is set by the number of cardiac cycles necessary to acquire one single 2D or 3D data set times the oversampling factor. The efficiency of the acquisition is defined by the number of lines accepted within the reconstruction gating range over the number of heartbeats required to complete the oversampled data set.

With this approach, Li et al. reported 3D MRCA measurement in which coronary artery lengths visualized on healthy subjects were considerably longer than what was possible with comparable breath-hold 2D MRCA scans [20]. Clinical results in patients with CA are summarized in Table 1. Post et al. studied 20 patients with coronary artery disease, identifying 96 % of the proximal coronary arteries, but encountered a low sensitivity of 38 % and a specificity of 95 % for stenosis detection [45]. Müller et al. presented data on 35 patients with unpredicted success, reaching a higher sensitivity of 83 % and a specificity of 94 % [46]. Huber et al. [47] reported on 20 patients a sensitivity and a specificity of 73 and 50 %, respectively. VanGeuns et al. [48] found a sensitivity of 50 % and a sensitivity of 91 % in 29 patients. Many more studies have been performed since then because of the availability of this particular MRCA protocol in many systems worldwide and reports have been generated locally and internationally with their findings. High sensitivity has been achieved once studies with sub-optimal image quality are re-

Fig. 10 a–c. Cardiac triggered, breath-hold 2D segmented GRE MRCA in a healthy volunteer. **a** Orientation along the right coronary artery *(RCA)*. **b** Orientation through the aortic root. **c** Orientation along *LM* and *LAD*. Every slice was collected in 22 heartbeats with a time resolution of 150 ms per shot (TR/TE = 13.7/6.7 ms, 11 lines/shot, 3 mm, 240 × 512 matrix, FOV = 285 × 380 mm^2). Compare these results with those of fast SE in Fig. 7. *LM* left main; *LAD* left anterior descending; *Ao* aorta; *RVOT* right ventricular outflow track

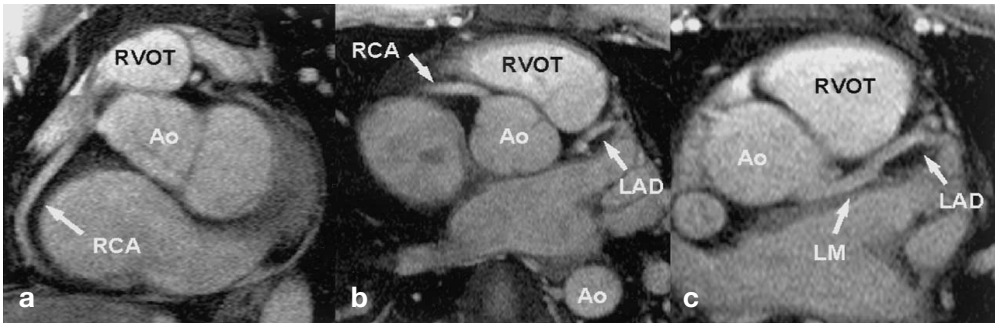

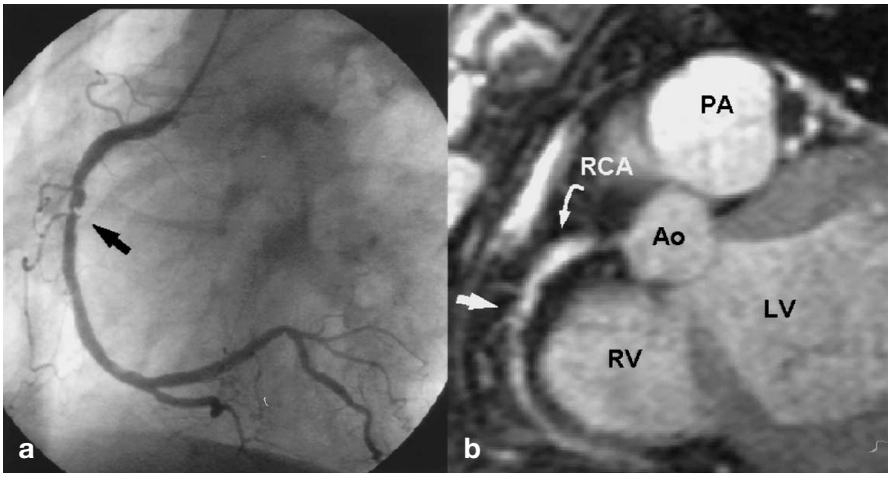

Fig. 11 a, b. Patient with stenosis in the mid-segment of the right coronary artery. **a** Conventional coronary angiogram. **b** Breath-hold 2D segmented GRE (turbo FLASH) image. Signal attenuation is reminiscent of the stenosis visualized in *CA (arrows)*. Improved spatial resolution and thinner slices are necessary to evaluate the high-grade stenosis. Fourteen heartbeats were used to scan a 154×256 matrix, slice thickness of 3 mm, 1.25×1.00 mm^2 in-plane resolution (other sequence parameters as in Fig. 10). *Ao* aorta; *RCA* right coronary artery; *RV* right ventricle; *LV* left ventricle; *PA* pulmonary artery (figures reprinted from Wielopolski PA, et al. (1998) Coronary arteries. Eur Radiol 8: 873–885)

Fig. 12 a–c. Collection of diaphragmatic excursion using a navigator signal. The navigator signal is generated from a spin echo using a typical SE readout with a rhomboidal cross section after the intersection of a sagittal slice defined by 90° RF pulse with an oblique slice generated by a 180° RF pulse. **a** Coronal scout image. **b** Transverse scout image. **c** Resulting diaphragmatic motion collected over 30 s with sampling occurring with the navigator echo collected every 240 ms. A respiratory excursion window is assigned where edge detection processing is defined over the region (to save processing time). The navigator data is attached to each data collection event in the cardiac period. The navigator data can be used retrospectively to sort the data or prospectively to make decisions in real-time on data acceptance with a predefined gating acceptance window (e. g., ± 1, ± 3, or ± 5 mm). Selected data lines lying within the desired gating window are depicted with *brighter circles*

moved from the evaluation. With successful data collection coronary stenosis can clearly be seen (Fig. 14). Image quality is still problematic even in cooperative individuals, as revealed in a study by Stehling et al. [49] on young healthy volunteers.

The prospective navigator-gated acquisition tracks the diaphragmatic position with a navigator over the diaphragm (or close to the target coronary, e. g., the wall of the left ventricle for the left coronary system) similarly as in the retrospective approach. However, real-time decisions are made to accept the incoming data during mid-late diastole when sampling is performed within the desired gating window rather than oversampling to encompass the entire respiratory waveform, as previously mentioned. The approach is considered to be similar to gating the acquisition with respiratory monitoring belts used for abdominal imaging (introduced a decade ago). Two-dimensional MRCA scans using prospective navigator gating with comparable quality to breath-holding were demonstrated by Oshinski et al. [21]. Scanning time is dependent on the gating window specified (smaller windows produce sharper results but scan time may increase substantially). An additional improvement that ameliorates efficiency has been evaluated by "re-registering" the volume scanned based on the

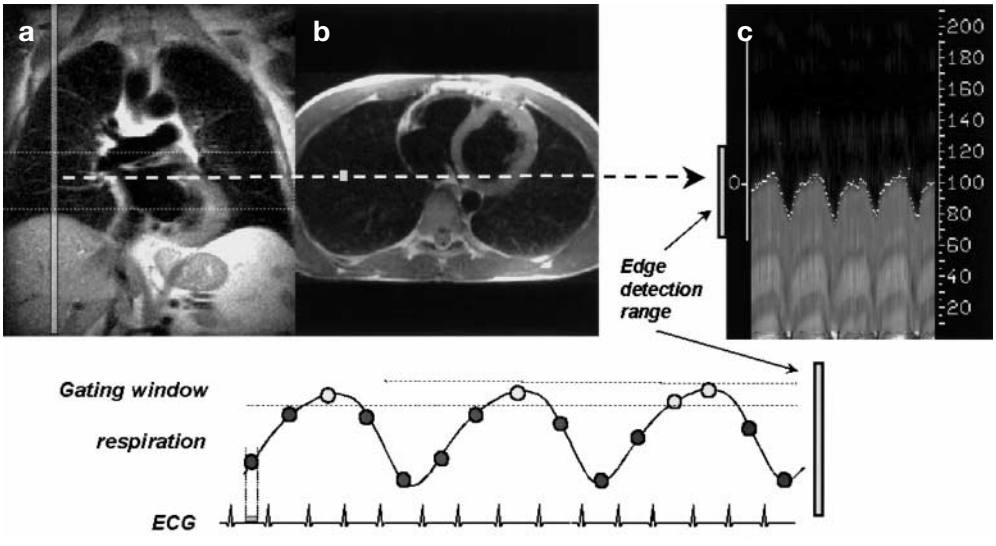

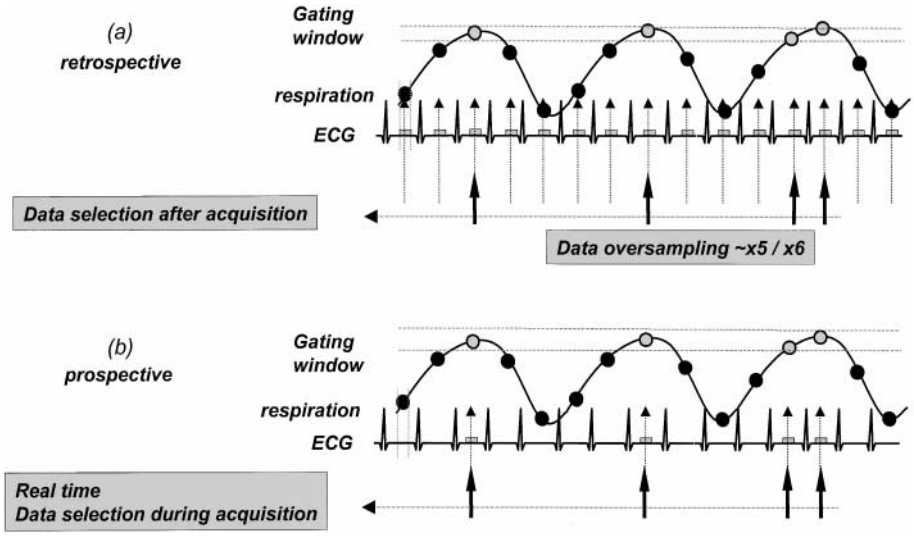

Fig. 13 a, b. Retrospective and prospective navigator MRCA data collection and processing schemes. **a** In retrospective navigator MRCA multiple cardiac triggered data sets are collected (oversampling by five to six time) to make sure that valid data exist during the entire respiratory period that match the criteria for data selection during reconstruction within a defined small acceptance window (e.g., ± 1, ± 3, or ± 5 mm). **b** In prospective navigator MRCA only those lines of data synchronized with the ECG that were collected within a predefined gating acceptance window are used for the reconstruction. Gating acceptance window in prospective navigator scanning can be variable to increase scanning efficiency (e.g., ± 1 mm at the center and ± 5 mm towards the edges of k-space). Retrospective navigator data collection requires enough computer memory to hold the multiple data sets (e.g., six times more for an oversampling factor of 6); nevertheless, the acquisition time is fixed to the number of heartbeats required to collect the complete set. Selected data lines are depicted with *brighter circles* in both cases

position indicated by the navigator. Using this idea, Danias et al. [31] demonstrated equivalent data to breathhold 2D acquisitions with a 33 % improvement in scanning efficiency (using a 3-mm window) when compared with navigator gating without position correction. Reported clinical studies using this technique do not abound and soon reports are to be expected. A recent study by Lethimonnier et al. on 20 patients revealed a sensitivity and specificity of 65 and 93 %, respectively [50]. Additionally, a small study reported by Stuber et al. [25] illustrates excellent image quality in healthy volunteers and good correlation with CA in 7 patients with coronary artery disease.

Other schemes are available to increase scanning efficiency even further. Jhooti et al. [51] have proposed the use of centrically ordered acquisitions in which the central portion of k-space is collected with a small respiratory gating window (e.g., ± 1 mm) while the data for the outer portions of k-space are scanned with increasingly coarser gating windows (e.g., ± 3, ± 5, and ± 7 mm). This group claims that image quality is not harmed significantly with such procedure while scanning efficiency can be increased to 50 %. They also affirm that consistently better image quality is obtained when compared with the retrospective navigator setup described above. The same group in a report by Yang et al. [52] investigated a 3D focused imaging approach using a volume-selective RF excitation (e.g., exciting a small cube volume of tissue inside the thorax containing only a coronary segment). The group refers to this technique as 3D zonal EPI MRCA, making it possible to concentrate on imaging only the coronary artery while achieving good image quality even with an extra 30 % reduction in imaging time.

The data quality with retrospective navigator MRCA approaches has been random even in healthy volunteer studies, as noted previously [49]. This has been shown experimentally by Jhooti et al. [51] investigating several schemes to compensate prospective navigator data collection while analyzing the possible pitfalls of the retrospective navigator approach. The group concluded that image quality was in direct relation to the goodness of the acquired data during the central portion of k-space. This investigation bears similarities to previous work on respiratory compensation schemes to reduce ghosting artefacts and increase scanning efficiency for free-breathing abdominal imaging such as reordered phase encoding (ROPE) and other schemes [53]. The addition here is the free choice of the gating acceptance window over different portions of k-space, thus controlling (predefining) the blurring function over the coronary vessels. A direct improvement of the retrospective navigator approach can be envisioned based on the same approach by making the constant oversampling factor used until a variable one is presented according to the region of k-space scanned. This requires further study and it is likely to increase imaging time substantially. The incorporation of segmented EPI readouts in retrospective and prospective navigator MRCA is likely to shorten scan time while maintaining good SNR and increased spatial resolution [54, 55].

Another interesting free-breathing approach that is claimed to be robust was introduced recently by Hardy et al. [56] striving for high-resolution coronary images using adaptive averaging. The method is based on cross correlation of real-time acquired frames and selective

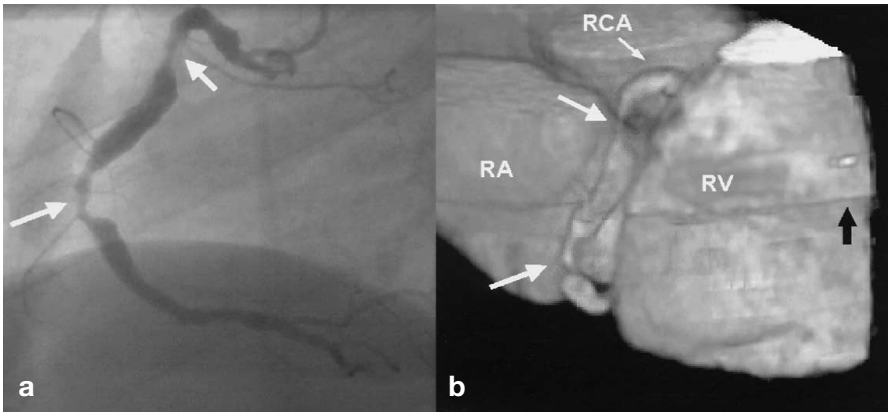

Fig. 14 a, b. Retrospective navigator 3D MRCA scan. **a** Conventional coronary angiogram. **b** Volume rendering of the RCA. *Straight arrows* indicate two stenoses located in the proximal and mid-RCA segments. Two slabs were collected with 24 2-mm-thick slices with a FOV of $280 \times 320\ mm^2$ and a matrix of 128×256, TR/TE = 7.4/2.7 ms, time resolution of 150 ms, and data collection time of approximately 25 min. The *black arrow* in **b** demonstrates a boundary artefact that identifies the extent of each slab scanned. *RCA* right coronary artery; *RA* right atrium; *RV* right ventricle (with permission from ref. 48)

averaging of those frames that contain a coronary segment in the selected imaging plane and at the proper location.

Third-generation MRCA: breath-hold volumetric MRCA with multislice 2D and 3D techniques

The trend in third-generation MRCA techniques is to acquire a volume data set in a single breath-hold. Breath-hold length, resolution, and coverage are balanced to obtain in several attempts a complete study of the coronary arteries. Although breath-hold volumetric techniques have been attempted previously with limited resolution [3], higher resolution and speed is possible with advanced gradient hardware. This was first investigated by Wielopolski et al. [10] using a breath-hold 3D segmented EPI approach. More recently, the addition of partial Fourier processing has shortened scanning times making it possible to cover the entire heart in one single breath-hold [26].

Because the 3D information is readily available after one breath-hold, MPR can be used to obtain optimal plane orientations that contain the coronary arteries and apply these for higher-resolution 2D and 3D scans that target specifically each coronary segment. This logic has been followed (dubbed VCATS for volume coronary arteriography with targeted scans) for the evaluation of a breath-hold 3D GRE sequence incorporating partial Fourier scanning to provide contiguous slices and immediate operator feedback (Fig. 16). Short examination times are therefore possible, taking as few as seven breath-holds to screen the entire coronary tree with comparable imaging times and image quality to single-slice breath-hold 2D MRCA (Figs. 17, 18). Despite the limited resolution that is possible in a short breath-hold with a limited number of heartbeats, signal non-uniformities and stenosis greater than 50 % can be visualized easily when breath-hold is adequate during the acquisition (Figs. 19, 20). Initial clinical results reported by Van Geuns et al. [57] on 34 patients with 31 coronary lesions ($\geq 50\,\%$ stenosis) found sensitivity and specificity values of 68 and 97 %, respectively. Other approaches consider volumetric imaging using breath-hold multislice 2D seg-

Fig. 15 a–c. Examples of prospective navigator 3D MRCA. **a** Curved multiplanar reformation along the LAD of a 42-year-old patient with chest pain but without coronary artery stenoses. **b** Patient with a tubular stenosis of the LAD coronary artery corresponds nicely with CA **(c)**. A T2 prepared sequence was used with TE_{eff} = 50 ms, 8 lines/shot with TR/TE = 7.4/2.5 ms (60-ms time resolution), 10 slices of 3 mm (interpolated to 20) scanned with a FOV of $305 \times 360\ mm^2$ and a matrix of 304×512. *RCA* right coronary artery; *LM* left main; *LAD* left anterior descending; *Ao* aorta; *RVOT* right ventricular outflow track. (Courtesy of W. Manning, Beth Israel Deaconess Medical Center, Boston, Mass.)

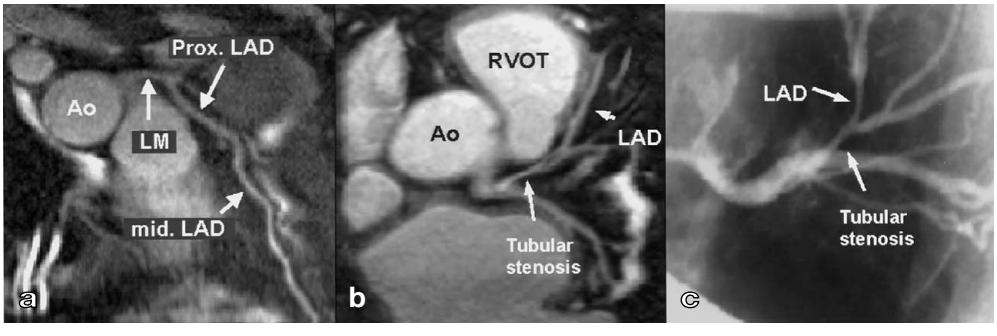

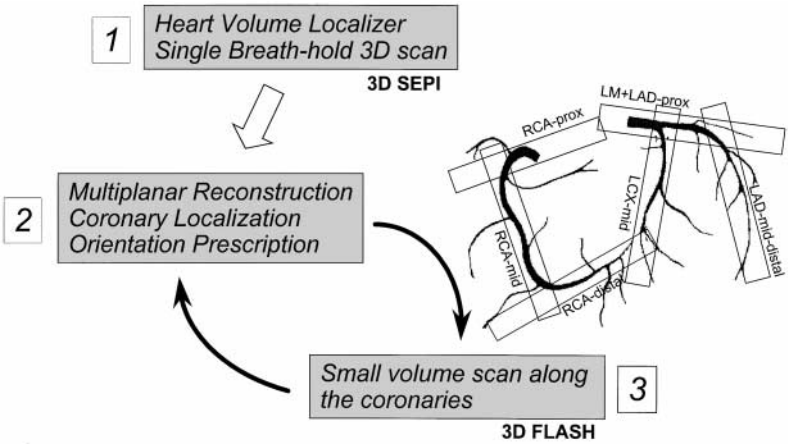

Fig. 16. One possible setup for fast coronary assessment using breath-hold 3D MRCA scans. *1* Using improved gradient hardware a volume localizer can be collected (e. g., using segmented 3D EPI scans) which provides enough spatial resolution in all directions to localize all plane orientations for coronary segments of interest (after multiplanar reformation) for targeted 3D MRCA scans *(2, 3)*. Breath-hold targeted scans can be set from the multiplanar reformation platform directly to acquire each coronary segment (interactive mode) or all orientations are pre-recorded first prior to scanning all coronary segments at once (sequential mode)

mented GRE [58] as well as spiral [28] and segmented EPI [27].

Ultrashort TR 3D contrast-enhanced MRCA with increased volume coverage has been increasingly evaluated to counteract the poor SNR of high-bandwidth acquisitions with a dynamic injection of short T1 contrast agent [59, 60, 61] has produced relevant clinical results on 30 patients with a sensitivity of 77 % and a specificity of 94 %. With the ability to use fluoroscopic triggering, rather than using a bolus test prior to scanning, should increase the consistency of the results using contrast-enhanced MRCA and produce optimal contrast, as shown recently by Li et al. [62]. To help patients to maintain a better breath-hold or to elongate the breath-hold period, the administration of oxygen during the preparation phase is helpful to ensure a successful study [63].

Fig. 17 a, b. Breath-hold targeted-volume MRCA (VCATS) along the aortic root orientation in a healthy volunteer. **a** Collage of 16 from 20 reconstructed slices. **b** Volume rendering shows the RCA and proximal LAD and LCX. Data collection performed during breath-holding in 21 heartbeats reconstructing 20 slices (7 scanned, 3 mm thick) using a 126 × 256 partial Fourier matrix, FOV = 220 × 290 mm^2, 21 lines/shot with TR/TE = 4.8/2.0 ms (100-ms time resolution). Magnetization transfer contrast (MTC) is applied prior to data collection on every heartbeat. Compare to breath-hold single-slice 2D MRCA of Figs. 7 b and 10 b. *Ao* aorta; *RCA* right coronary artery; *LM* left main; *LAD* left anterior descending; *GVC* great cardiac vein

Additional applications of MRCA

Coronary artery anomalies

Anomalous origins of coronary arteries appear in approximately 1.2 % of patients referred for CA [64]. In the majority of cases it is benign in nature, but may be

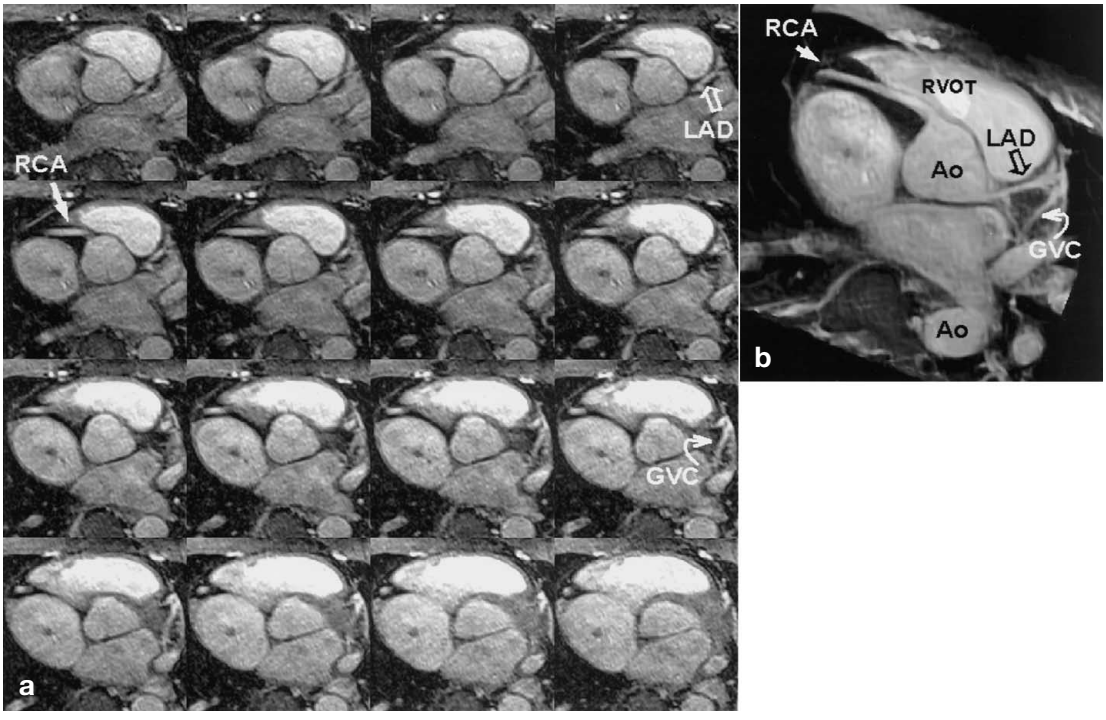

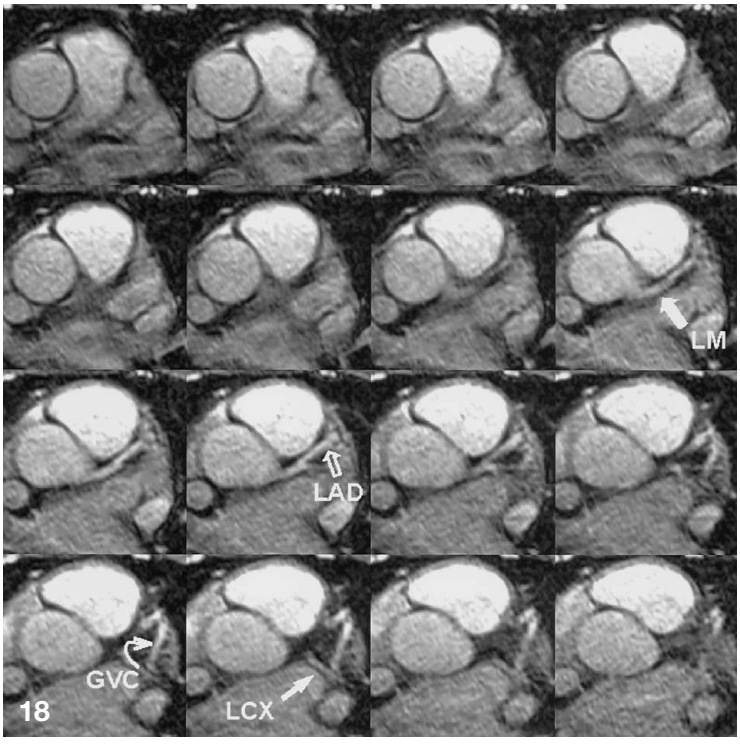

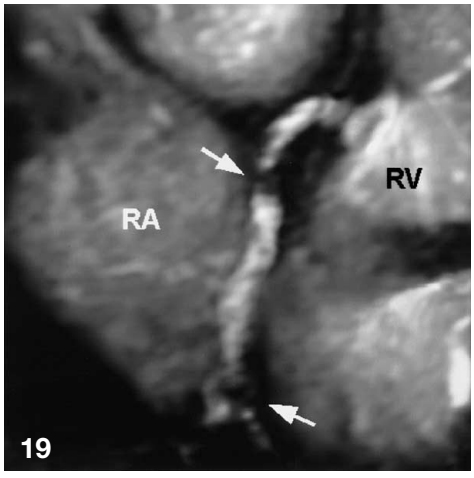

Fig. 18. Transverse targeted-volume MRCA (VCATS) at the level of the left main *(LM)*, clearly depicting LM, left anterior descending *(LAD)*, and left circumflex *(LCX)* coronary arteries. Compare with breath-hold 2D MRCA of Figs. 7c and 10c. Imaging parameters as in Fig. 17; *GVC* great cardiac vein

Fig. 19. Volume rendering of a VCATS tangential to the mid-RCA segment collected on the same coronary patient as shown in Fig. 14. The example shows clearly the two stenotic segments *(arrows)*. Imaging parameters as in Fig. 17. *RA* right atrium; *RV* right ventricle

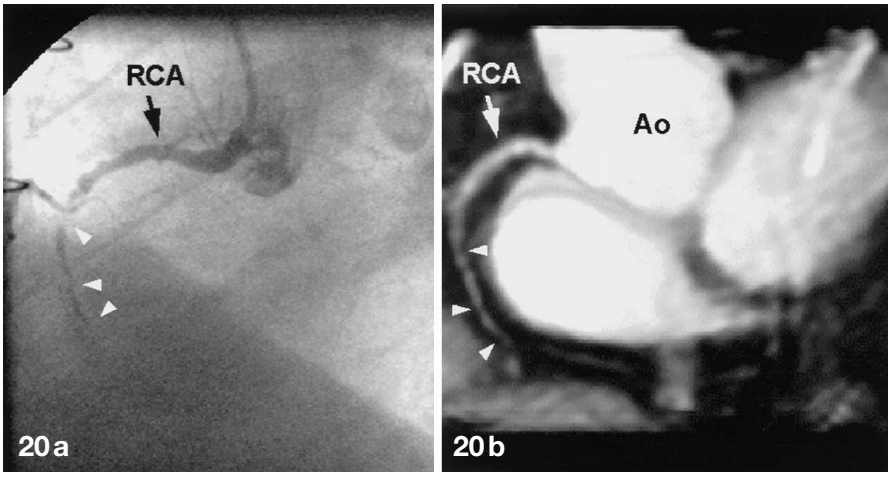

Fig. 20. **a** Conventional coronary angiogram in a patient demonstrating diffuse coronary artery disease along the RCA. **b** Volume-rendered image of VCATS collected along the RCA demonstrates signal variations corresponding closely to those seen in CA. *Arrowheads* demarcate equivalent locations in both. Imaging parameters as in Fig. 17. *RCA* right coronary artery. *Ao* aorta

the cause of sudden death [65, 66]. Detection of these anomalies can be performed with any MRCA technique available, as it has been proven that MRCA is highly effective for this indication and can be regarded as a definite tool for the diagnosis [67]. Additionally, it can be advantageous over CA in cases with inconclusive results [68]. Two blinded studies using MRCA involving 35 patients have identified the anomalous coronary artery and its course in 97% of cases [67, 68].

Assessment of coronary artery bypass graft patency

Coronary artery bypass grafts have lesser mobility with cardiac and respiratory motion and also have a larger lumen (5–10 mm) when compared with native coronary arteries. This has made it possible even for conventional SE and GRE techniques to show some success in their evaluation [69, 70, 71, 72, 73]. Obstacles to CABG imaging are set mainly by local image artefacts (geometric distortion and signal loss) associated with nearby metallic homeostatic clips, sternal wires, and graft markers. This has been particularly problematic for imaging internal mammary artery bypass grafts, which is the reason that they have been visualized only in a limited number of patients.

With SE techniques, a patent or occluded graft is diagnosed after observing signal loss or prevalence of the graft lumen. In an early investigation by White et al. [74], a sensitivity and a specificity of 86% and 59%, respectively, were reported. However, remnant signal in cases of stenosis from slow-flowing blood could lead to false negatives. With increasing experience and the incorporation of cine GRE techniques, many investigators obtained improved sensitivity and specificity for by-

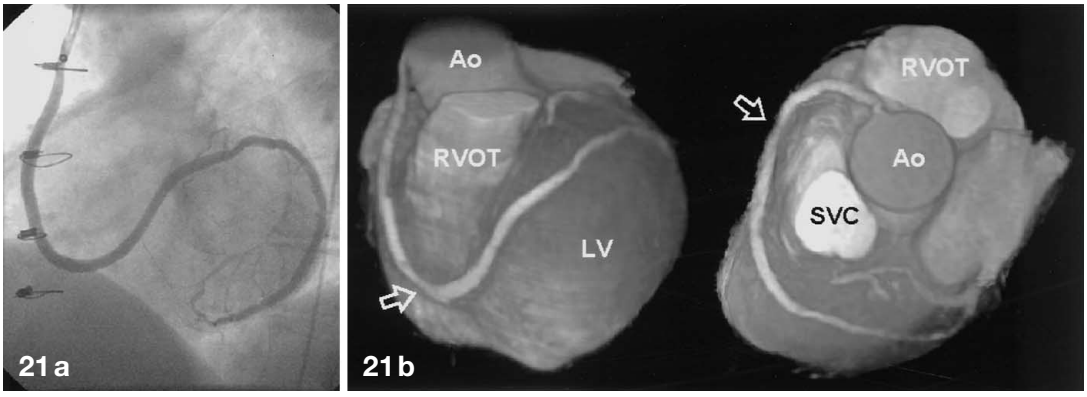

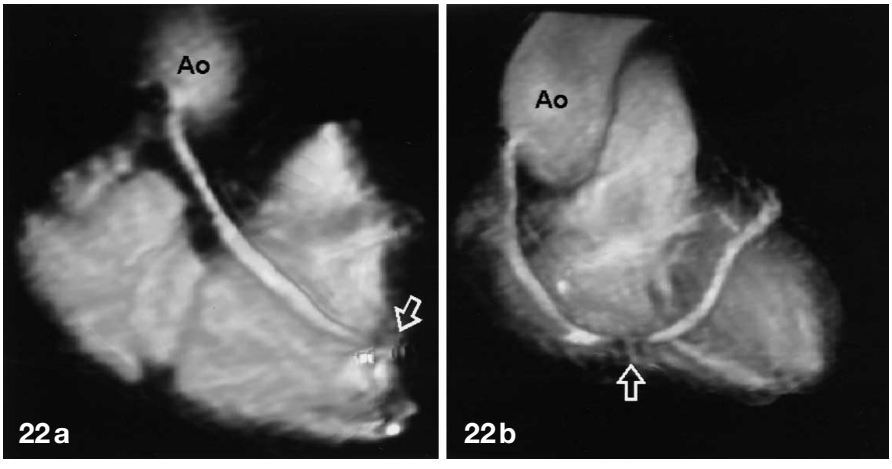

Fig. 21. a Another CA view of the same venous jump coronary bypass graft as demonstrated in Fig. 8. **b** Two volume-rendered views of the retrospective navigator 3D MRCA scan demonstrate the entire course of the coronary artery bypass grafts (CABG) from the aorta crossing over the right ventricular outflow track *(RVOT)* towards the left anterior descending artery. The *two arrows* indicate the location close to the sternal wires that create some artefactual lumen thinning. Two 64-mm slabs were collected with 64 2-mm-thick slices per slab (32 scanned) with a FOV of 280×320 mm^2 and a matrix of 128×256, TR/TE = 4.8/2.3 ms, time resolution of 154 ms, and data collection time of approximately 28 min. Magnetization transfer contrast preparation and administration of an intravascular-like/liver contrast agent (Endorem, Guerbet, Paris, France) were included to increase contrast between myocardium and blood. Note the signal attenuation from the surface coil towards the end of the graft. *Ao* aorta; *LV* left ventricle; *SVC* superior vena cava

Fig. 22 a, b. Two VCATS examples using two planes to depict a large portion of the venous jump CABG on the same patient as in Fig. 21. Note that a similar stenosis arises from the proximity of the sternal wires *(arrows)*, more accentuated in this case due to the slightly larger voxel acquired and a partial Fourier reconstruction. Scanning parameters as in Fig. 17. *Ao* aorta

pass patency but did not look into the presence of stenosis (see Table 2) [75, 76].

Using retrospective navigator 3D MRCA, Kessler et al. reported the results on 7 patients with CABGs within a large study on coronary artery stenosis detection, correctly classifying 4 occluded and 13 of 15 patent grafts (Fig. 21) [77]. Breath-hold acquisitions are becoming more popular because of increased examination speed and patient comfort. Using breath-hold contrast-enhanced 3D GRE imaging, Vrachliotis et al. [78] and Wintersperger [79] also demonstrated the high sensitivity and specificity of the contrast-enhanced approach. However, the length of the acquisition window per cardiac cycle (300–500 ms) introduces blurring of those CABG segments close to the heart impairing diagnosis of stenosis. Some CABG studies have been performed that do not require the administration of contrast, as previously shown with breath-hold 2D MRCA [80] and more recently with thin slab 3D breath-hold scans (Fig. 22).

A report combining both breath-hold black-blood fast SE (HASTE) and contrast-enhanced 3D imaging was performed recently by Kalden et al. on 22 patients (59 grafts) [81]. Black-blood HASTE provided 95 % and 93 % for sensitivity and specificity for detection, respectively, with similar results for contrast-enhanced 3D angiography (94 %). The shorter acquisition in black-blood HASTE sequence could reveal better patent distal graft anastomoses. A relevant example of this technique is shown in Fig. 8.

Discussion

Coronary visualization

Presently, the coronary arteries can be routinely visualized with many MRCA techniques; however, drawbacks inherent to MRI must be considered that can significantly impair image quality and diagnosis. Typical non-

Table 2. Sensitivity, specificity, and accuracy of various techniques in the assessment of coronary artery bypass graft patency as compared with conventional coronary angiography. CE 3D GRE refers to contrast-enhanced 3D GRE scanning during dynamic bolus contrast injection. *HASTE* half-Fourier acquired single-shot turbo spin echo

Reference	Technique	No. of grafts	No. of patent grafts	Sensitivity (%)	Specificity (%)	Accuracy
2D techniques						
White et al. [69]	SE	72	50	86	59	78
Rubinstein et al. [70]	SE	47	29	90	72	83
Jenkins et al. [72]	SE	41	26	89	73	83
Frija et al. [73]	SE	52	43	98	78	94
Galjee et al. [75]	SE	98	73	98	85	96
White et al. [74]	Cine-GRE	28	14	93	86	89
Aurigemma et al. [76]	Cine-GRE	45	33	88	100	91
Galjee et al. [75]	Cine-GRE	98	73	98	88	96
Kalden et al. [81]	2D HASTE	59	44	95	93	95
3D techniques						
Vrachliotis et al. [78]	CE 3D GRE	44	29	93	97	95
Wintersperger et al. [79]	CE 3D GRE	76	60	95	81	92
Kalden et al. [81]	CE 3D GRE	59	44	93	93	93

contrast enhanced bright-blood MRCA suffers from the same common ailments. Fat suppression (or selective water excitation) is performed to obtain the high contrast necessary to observe the coronary arteries surrounded in most of their course by pericardial fat. Fat suppression can be cumbersome to achieve over the entire heart or the thorax because of the extensive presence of air–tissue interfaces and also from the possible presence of neighboring metallic objects such as sternal wires. The geometry of the heart and the thorax also plays a role in defining a region of good magnetic homogeneity, but this issue has yet to be addressed adequately (e. g., long vs short thorax). Most likely some coronary segments will be problematic to image and localized shimming per region of interest will be necessary to ensure homogeneous fat suppression.

Coronary arteries cannot be visualized well if SNR is poor. Low-bandwidth readouts, of the order of 100–200 Hz/pixel for 2D MRCA, are used to counteract poor SNR. Nonetheless, fat chemical shift can produce enhancement or attenuation in the coronary arteries and surroundings with poor fat signal reduction. Particular choices of TE that lead to an opposed-phase behavior for fat (producing periodic reductions in its signal, e. g., at TE = 2.38 ms, TE = 7.14 ms, for 1.5 T) can help to increase contrast and to delineate the coronary vessel. Yet, a signal cancellation at fat–vessel boundaries always occurs and low-resolution scans can introduce artefactual vessel thinning leading to a false stenosis (e. g., coronary segments of the order of one pixel may appear as black lines).

Another issue is the sensitivity of a technique to provide good resolution and adequate contrast for stenosis detection. In general, 2D MRCA uses long TE. Long TE can help in the detection of high-grade stenotic regions ($> 70\,\%$) by leaving a small signal void trace that can be used as an indicator to a problematic region when resolution is not adequate (large voxel sizes). Generation of signal voids at longer TEs is not precisely desired, but the additional contrast between vessel wall or plaque and vessel lumen that could be obtained for enhanced differentiation is. At short TE, plaque may be indistinguishable from vessel lumen even in cases of stenosis. A downside to the better contrast is that longer TE slows down data collection because of increasing TR. Geometric distortions and signal loss induced by poor magnetic field homogeneity created by metallic materials, such as stents, sternal wires, etc., can obscure a coronary vessel (or CABGs) completely, requiring the use of shorter TE. Therefore, the issue of TE selection is a cumbersome one, and as a result of the gradient hardware improvements that lead to faster data collection, TEs between 1.8 and 2.7 ms are selected just to obtain the opposite-phase behavior of fat and a short TR while contrast enhancement between plaque and wall and coronary lumen is generated using the previously discussed MT preparation schemes or T1-sensitive sequences after administration of contrast agents.

Black-blood MRCA techniques (East SE based, 2D and thin-slice 3D), as shown in Fig. 7, can be considered robust when looking at all problems described herein. Only cases with slow blood flow might be considered difficult to interpret. Nevertheless, the appearance of vessel lumen signal indicates that velocities may be abnormal and attention should focus in that region.

Interpretation difficulties

Primarily, SNR limits the effective spatial resolution achieveable with 2D and 3D breath-hold MRCA. Breath-hold 2D MRCA requires considerable experience in making the correct assumptions in potentially problematic regions to recognize real from artefactual information. The localization of focal coronary stenoses can only be indirectly perceived through signal fluctuations along the vessel path created by flow dephasing arising from turbulent flow behavior. However, false stenoses may be induced during the review process in cases of tortuous coronary arteries and poor breath-hold reproducibility. Blood-signal saturation could be used as an indicator to poor blood-flow refreshment or complete occlusion, but this does not play a significant role for stenosis detection (see further on the issue of

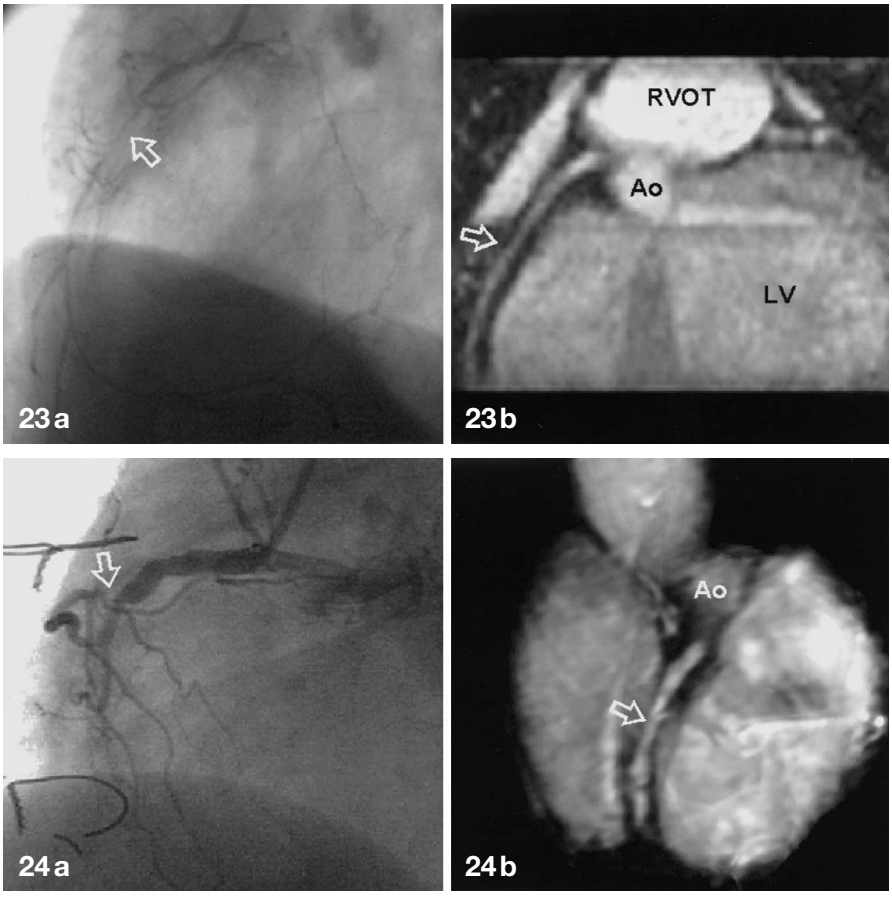

Fig. 23a, b. Patient presenting a complete occlusion of the RCA on CA (**a**) appears as normal after multiplanar reconstruction analysis of a retrospective navigator 3D MRCA scan (**b**). *Arrow* in **a** points to a severe narrowing of the RCA, not seen clearly in **b** despite good image quality but with a slight but noticeable decrease in signal intensity. Scan parameters as in Fig. 14. *Ao* Aorta; *RVOT* right ventricular outflow track; *LV* left ventricle

Fig. 24a, b. Another example of severe disease of the RCA comparing CA (**a**) with a volume-rendered image of a breath-hold VCATS collected tangential to the mid-RCA segment (**b**). While CA demonstrates an abnormal course with multiple stenotic regions after the first right ventricular branch *(arrow)*, VCATS illustrates a vessel with abnormal signal indicating the presence of disease but with misleading lumen size. This may be consequent to remnant signal from plaque and coronary vessel wall in a scan which is mostly proton-density weighted. Scan parameters as in Fig. 17. *Ao* aorta

dynamic imaging) unless scans are performed perpendicular to the vessel path to enhance inflow effects.

Other interpretation difficulties can arise. Heart motion, beat-to-beat variations, or poor breath-hold can significantly blur vessel detail. Differentiation between arteries and veins can be difficult, especially between the LAD and LCX from the great cardiac vein in distal segments [82]. The pericardial sac can appear as a linear structure with medium to high signal intensity similar to a coronary artery. Fluid in the superior pericardial recess (running posterior to the aortic root) may show as a linear structure joining the proximal LAD, making it appear as a continuation of the vessel itself. All these difficulties have been reviewed in depth by Duerinckx et al. [83] for 2D MRCA and are equally applicable to any non-contrast-enhanced bright-blood MRCA technique.

Role of dynamic imaging

Unfortunately, non-contrast-enhanced MRCA may not be as reliable an examination as initially envisioned even with perfect fat suppression and advanced gradient and signal reception hardware. As mentioned previously, non-contrast-enhanced MRCA can be considered mainly a proton-density-weighted examination for all tissues, but the signal from chemically shift suppressed fat. The reason for having a proton-density-weighted contrast is a direct consequence of the wait interval introduced by the cardiac synchronization necessary for each segment of data collected. Therefore, the signal from stagnant blood, blood clot, or plaque can recover completely and appear as integral part of coronary artery (appearing isointense), especially when SNR and resolution are not sufficient or adequate. This creates a difficulty in interpretation because of poor tissue discrimination, as exemplified in Figs. 23 and 24 from our experience, also noted by others [84], using thin-slab 3D MRCA scans and 2D MRCA with vessels in the plane of section. This is the reason why for 2D MRCA, stenosis could be better seen with additional 2D thin slices acquired perpendicular to the coronary artery lumen [38, 39]. The use of magnetization-prepared contrast in the form of MTC or T2 preparation can be helpful in such instances to produce the necessary differentiation, but this has yet to be shown.

To tackle this differentiation problem, enhancement of a coronary segment could be monitored more closely using some form of dynamic information, similar to what can be seen in CA. One way to achieve this is by using the intrinsic contrast possible by blood motion itself through blood-tagging MRCA techniques such as reported by Edelman et al. [85] and Wang et al. [86]. These techniques can tag selectively blood at the aortic root to observe blood moving into the coronary arteries after an appropriate delay between tag and imaging is selected. Subtraction is performed from an untagged

blood image, collected interleaved with the tagged one. This removes interfering fat and myocardium to produce an image of only tagged blood flowing into the coronary arteries. Tagging and inflow delay selection require some experience to visualize a large portion of the coronary arteries and image quality can vary substantially depending on the range of blood flow velocities present and the fraction of tagged blood that flows into the coronary arteries.

Dynamic imaging during the injection of a contrast agent using a short TR/TE T1-weighted 2D or small-slab 3D GRE or segmented EPI scan could provide a more adequate answer to the problem by providing better SNR and speed. By observing dynamically the enhancement of the vessels of interest, those vessels that are poorly enhanced or show noticeable discontinuities in their enhancement pattern are indicative of problems. The enhancement process is better observed after subtraction of a pre-contrast frame. One of several reports has investigated the role of a 2D projective-subtraction method [87].

Future directions

Dedicated MR cardiac scanners

The majority of MRI manufacturers of high-field systems now offer dedicated cardiac scanners with strong imaging gradients (> 30 mT/m) and fast rise times (> 150 mT/m per millisecond) optimized for a smaller effective imaging field of view to provide speed with a higher peripheral nerve stimulation threshold. The ever-increasing addition of an arsenal of measurement tools may soon prove to encompass all that was always envisioned for an integral evaluation of the heart and the coronary arteries. These tools include real-time capabilities with interactive platforms for measurement setup (including 3D steering devices) and evaluation [88, 89, 90, 91]. The implementation of parallel imaging strategies that dramatically shorten image acquisition times per cardiac frame may also become available on all these systems [92]. This would make it possible to evaluate the heart function and perhaps the coronary arteries with exquisite temporal resolution (not requiring ECG triggering) and spatial resolution that rivals that of ultrasound both in flexibility and image quality. This may bypass some of ultrasound's measurement disadvantages such as finding a good acoustic window, ultrasound beam attenuation, and obstacles as with chest wall interference and intervening pulmonary parenchyma [93].

Yet some issues must be addressed before dedicated scanners enter routine clinical practice for MRCA. Breath-hold or free-breathing MRCA (or a combination of both) is still under debate to solve in a reliable and time-efficient fashion the majority of coronary cases. At this moment improvements in slice-position correction methods and special encoding schemes in free-breathing MRCA using prospective navigator gating seem sufficiently robust to adjust to every type of respiratory motion pattern and permit adequate resolution for stenosis evaluation. Research in many institutions and innumerable modifications to current MRCA techniques have marked a pace in the past 2 years to search for that reasonable balance between available and future improvements.

Another important point is to provide the appropriate SNR–scanning time relationship to achieve the target resolution for stenosis quantification in short imaging times. The SNR is still a problem for high-resolution imaging at 1.5 T with phased-array coil technology. The recent introduction of 3-T whole-body systems may mark an important step for MRCA in conjunction with the commercial introduction of intravascular contrast agents. Because of SNR restrictions, scanners may not require the faster imaging gradients now available but just an "intelligent" setup that optimizes scanning possibilities with currently available technology.

Processing power is still a major concern in current scanners, e.g., scans may take much longer to reconstruct than the actual data collection time (e.g., breath-hold scans of approximately 20 s taking a minute to process before review). It is clear, however, that real-time interactive MRI will set the new pace for enhanced system platforms with better processing speed, flexibility for dynamic display, volume rendering, and data evaluation. Nevertheless, we feel that soon enough cardiac MR systems will take shape to satisfy cardiologists and provide an easy setup and the acquisition flexibility that is current in ultrasound examinations.

Intravascular contrast agents

The dramatic T1 shortening possible in blood with dynamic injections of gadolinium chelates (< 50 ms) in combination with ultrafast GRE techniques has yielded high-quality breath-hold MRA. However, providing a specific concentration to obtain consistent T1 shortening in blood is difficult because it depends on many parameters (e.g., physiology and injection settings). Furthermore, for MRCA, a single breath-hold and injection may prove inadequate for complete coverage of the coronary tree. Examination success is also measured by patient cooperation.

Gadolinium (Gd) chelates and ultrasmall superparamagnetic iron particles (USPIO) as intravascular contrast agents are being tested with long blood half-lives (~ 1–2 h) with hopes of providing the long-awaited essential boost for MRCA [94, 95, 96, 97]. This includes agents such as Angiomark (MS-325, Gd-based, Epix Medical, Massachusetts, USA) and Clariscan (NC100150, Nycomed-Amersham, Oslo, Norway). However, it is difficult to draw conclusions about the present utility of these intravascular contrast agents which will soon enter the market if used for MRCA studies alone. Undoubtedly, the success of any intravascular contrast agents will happen once the barriers of contrast and SNR are achieved specifically for T1-weighted MRCA sequences with considerable suppression of the fat signal. This will only occur whenever the

T1 relaxation in blood comes close to 50 ms or less and preferably using a 3D imaging sequence.

The choice of contrast agent used, Gd-based or USPIO, should not matter for the application. Both types can reduce the effective T1 of blood to values < 100 ms; however, Gd-based agents are presumably more advantageous than USPIO contrast agents because they maintain a longer T2* in blood with similar T1 shortening, thus reducing the constraints over how short TE must be before signal from blood decays (a special consideration for EPI scans). Contrast agents, such as dysprosium or superparamagnetic iron oxide particles (SPIO) [98], can also be effective to shorten T2* even further and can be used for blood signal suppression in coronary arteries for black-blood imaging. It must only be taken into account that myocardial perfusion imaging may be a routine part of a coronary examination, and first-pass injection of a bolus of the contrast agent chosen should be possible.

In summary, the success of a contrast agent will be strongly coupled to the MRCA technique chosen. We must be consider three working regimes of vascular signal in bright-blood MRCA. Most of the scans usually performed for MRCA are proton-density weighted with the exclusion of the chemical shift fat-suppression pulse and any form of magnetization preparation (MTC, T2 prep). When inflow is present, blood signal for each data collection is completely recovered in the region of interest. In the case that no inflow is present, blood can recover substantially according to the time between the last RF pulse executed on the previous heartbeat and the first on the subsequent heartbeat.

For proton-density-weighted 3D MRCA scans with large-volume coverage, it is only necessary to achieve uniform chemical shift fat suppression over the entire heart, and that blood, recovers completely before acquisition occurs on every heartbeat. To speed up the magnetization recovery of blood the administration of already approved contrast agents, such as Endorem (Guerbet, Paris, France; Feridex, Advanced Magnetics, Massachusetts) or Gd-DTPA, can ensure a uniform signal recovery for blood in all vascular compartments (Fig. 25). For Endorem, the SPIO accumulates for 80–90 % in the liver and spleen [99], whereas a 10–20 % fraction remains intravascular with a mild T1 relaxation during steady state (T1 relaxivity ~ 400–600 ms) and a long half-life [100]. Such agent is not necessary for 2D or thin-slab 3D MRCA. The last regime is that of T1-weighted scanning, to which all comments stated at the beginning of this section apply in this case (Fig. 26). These three regimes have been well described and analyzed by Johansson et al., simulating achievable contrasts and SNRs possible for different T1 characteristics of blood [101]. We encourage the reader to explore this reference as it is of major importance in the understanding of the effect of contrast agents for MRCA.

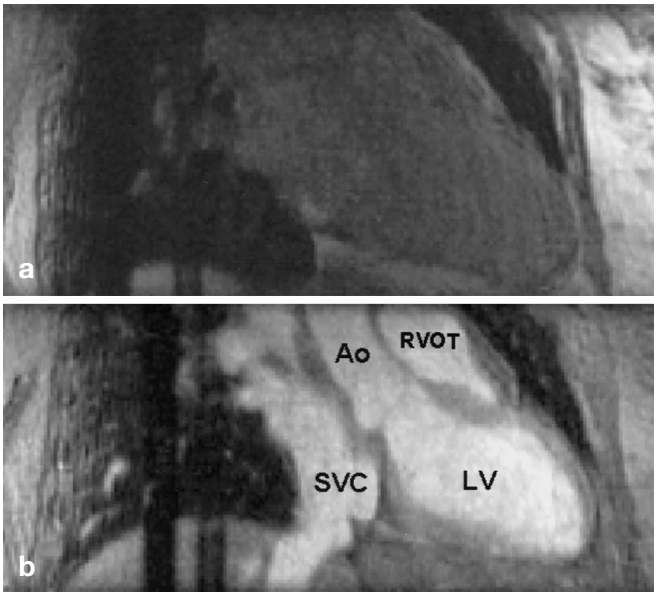

Fig. 25 a, b. With large volume scanning significant blood saturation occurs even with proton-density weighted contrast 3D MRCA scans with data collection on every heartbeat. A retrospective navigator MRCA was acquired covering the entire heart **a** prior to and **b** after administration of a liver contrast agent (Endorem, Guerbet, Paris, France), a large superparamagnetic iron-oxide particle (SPIO) contrast agent remaining approximately 10–20 % intravascular. The addition of Endorem makes signal from blood uniform in all blood-filled compartments and permits structure differentiation. *Ao* aorta; *RVOT* right ventricular outflow track; *SVC* superior vena cava; *LV* left ventricle

Cardiac triggering

Many cardiac examinations are hampered by suboptimal and inconsistent ECG triggering. Cardiac lead placement can be cumbersome in some cases and a good ECG trace is not guaranteed once the patient is moved into the magnet bore. Therefore, the setting process can be time-consuming if reposition is necessary and can take a considerable part of the cardiac examination time. Furthermore, with faster gradient switching ECG is frequently perturbed by voltages induced between the electrodes and on the cable-carrying signals between the electrodes and the ECG monitoring unit. This may cause possible mistriggering, threatening to produce bad-quality images especially in first-pass contrast-enhanced 3D studies using increased high-amplitude gradient activity. The perturbation is also sequence and orientation dependent.

One solution provided by some manufacturers is an ECG system in which certain derivation can be selected at will that produces the best ECG tracing. Nevertheless, this does not guarantee complete elimination of the interference created by the gradient switching and newly developed optical ECG devices have started to appear on the market [102]. These devices amplify the ECG signal close to the reception electrodes and send the analog signal via fiber optics to the patient-monitoring unit. These devices have proven robust even with EPI acquisitions [103] and will be available with future cardiac-dedicated MRI units. Another solution proposed by Vasanawala et al. [104] uses a more exotic approach mapping the velocity profile in the aorta using a velocity-sensitive navigator echo and producing a trig-

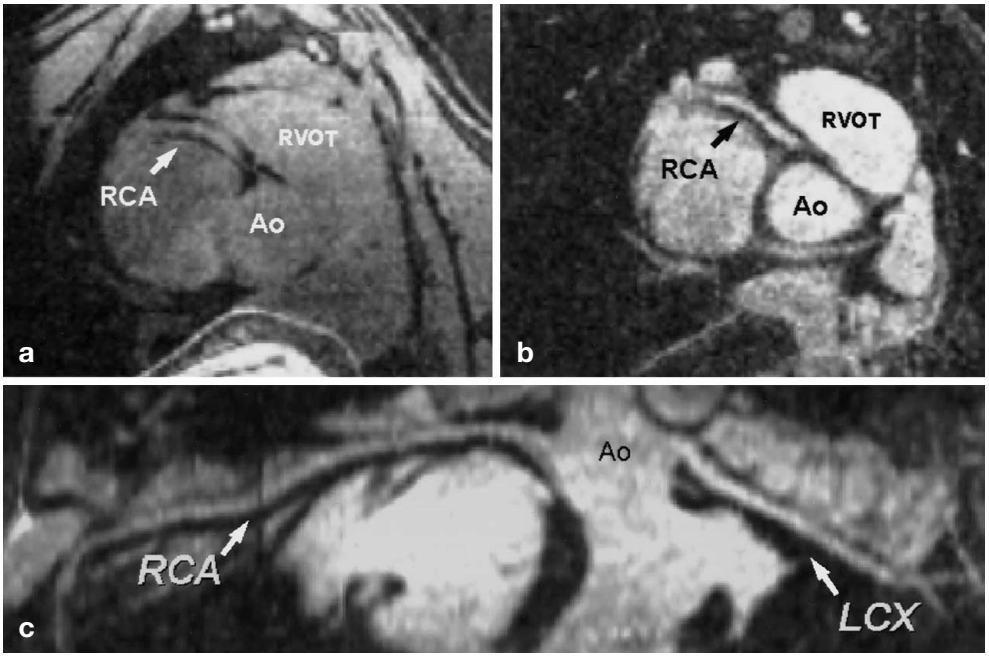

Fig. 26. a, b The effect of an intravascular contrast agent Gadomer-17 (Schering, Berlin, Germany) in improving visualization of coronary arteries in a pig. The left and right images were acquired before and after administration of Gadomer-17 (dose: 0.05 mmol/kg), respectively. A retrospective navigator 3D MRCA scan was used with a spatial resolution of $1 \times 1 \times 2$ mm^3. The SNR at the RCA was increased by a factor > 2 after contrast administration using an inversion pulse prior to signal acquisition to null the myocardium. **c** Curved multiplanar reconstruction of the contrast-enhanced data set, showing good delineation of both RCA and LCX. *Ao* aorta; *RCA* right coronary artery; *LCX* left circumflex; *RVOT* right ventricular outflow track. (Images courtesy of Dr Debiao Li, Northwestern University, Chicago, USA)

ger signal in real-time upon a predefined criterion in an interactive platform. A reproducibility study and quality assessment in comparison with the more conventional ECG triggering approach has proven consistent and has been judged to produce better overall image quality. The use of pulse monitoring can also be used to obtain better image quality in cases of mistriggering with standard ECG reception and processing.

Imaging of the coronary artery wall

A major challenge for MRI of the coronary arteries is to image the coronary artery wall. Coronary artery stenosis can arise from a stable atherosclerotic plaque which contains mainly fibrous tissue and calcium or a vulnerable plaque containing a large lipid core covered by a thin fibrous cap. This cannot be differentiated by CA and the vulnerable plaques are the ones that are important to detect as they are the reason that myocardial infarction occurs after the fibrous cup ruptures and a subsequent intravascular thrombus develops and blocks the coronary artery. The MRI and MRA techniques can contribute greatly by providing a more realistic picture of the problem and an answer to tissue characterization [105]. Unfortunately, SNR presently is not sufficient to visualize the coronary wall at high resolution in free-breathing examinations and less so for breath-hold acquisitions.

Attempts to produce coronary artery wall images have been presented by McConnell et al. [9] and Meyer et al. [28] using black-blood techniques. New developments in invasive MRI using intravascular catheter MR probes may overcome the SNR barrier now imposed to vessel imaging away from externally placed coils and provide some definitive answers to study more closely atherosclerosis [106, 107].

Parallel image-encoding techniques: fast techniques made ultrafast

Faster imaging is always possible by increasing the speed at which data is encoded. This is generally done by increasing readout bandwidth (stronger gradients) and minimizing gradient switching times to achieve shorter TRs (faster rise times). Nevertheless, the conventional sequential spin-warp phase-encoding process of one raw data line per readout event still proves to be the time-consuming process for extended coverage and resolution for MRCA scans. An additional speed-up factor can be achieved for any type of imaging sequence that uses spin-warp encoding (more recently studied for other k-space trajectories e. g, spirals) when multiple RF coils are used for signal reception. In principle, the idea is straightforward when bearing in mind that a coil has a limited reception region according to its specific coil sensitivity and can be precisely localized in space. It is this signal localization that can be used as an additional calculation variable to accelerate data acquisition.

The concept to use the inherent spatial location of a coil in an array to reduce acquisition time has been proposed previously; however, a more elegant and recent

redefinition of the concept has appeared under the acronyms SMASH (simultaneous acquisition of spatial harmonics) imaging [108]. The spatial localization of the coil reception pattern can be made inherent to the data collected, making it possible to parallelize the conventional phase-encoding process when the phase-encoding direction is chosen, e.g., along the long axis of the coil array. SENSE (sensitivity encoding), another way to accelerate acquisition using the same principle, uses a more general formulation to solve the problem that does not the require that coils be located along the phase-encoding direction as in SMASH [109].

The acquisition speed improvements offered by these parallel imaging techniques can be used in several ways, including constant resolution with shorter breath-hold times or improved resolution, otherwise with presently used scanning times [110].

Conclusion

Magnetic resonance coronary angiography has come a long way since the start of MR cardiac applications, reinforced by the fact that excellent images of the coronary arteries can be acquired. However, at this stage, no MRCA technique has yet fully proven reliable for coronary stenosis detection to be available for routine clinical work-up in the near future. The role of contrast agents for SNR and contrast enhancement is clear for contrast-enhanced MR angiography but does not yet provide the definite answer to reliability and reproducibility for MRCA. The introduction of dedicated MR cardiac scanners with high gradients and short rise times in conjunction with intravascular contrast agents with ultrashort T1 (of the order of 25 ms or less) may dictate the definite fate of MRCA in the coming years. Nevertheless, most MRCA techniques are still invaluable in clinical practice for a non-invasive, general view of the coronary system. The techniques can map the course of anomalous coronary arteries and question the patency of coronary artery bypass grafts and has proven to be a valid screening tool in young patients with unexplained arrhythmias or syncope during exercise. At present, second-generation MRCA techniques are still under scrutiny but with a clear tendency to favor prospective navigator rather than retrospective navigator MRCA. Third-generation MRCA techniques are making their way to trials with stronger and fast imaging gradients, and may soon appear in trials linked with intravascular contrast agents. We conclude that it is still the practical goal of any MRCA technique to be reliable enough to provide a "true" isotropic resolution with 1-mm^3 voxels for any coronary segment of interest. With adequate contrast, this resolution should make it possible to visualize hemodynamically significant stenoses.

Internet links to cardiac-related sites

Scientific communication is becoming increasingly popular using the World Wide Web (WWW) as a means to stay informed on the happenings around the MR cardiac community. Some institutions have made their internal websites public to illustrate ongoing research in the field of MRCA and related topics. Many locations exist with scattered data that can be accessed using key words such as, e.g., "coronary MR angiography" or "cardiac MRI" in the input of the many available web search engines. The URL that we found that is of special interest on the current image quality achievable with MRCA and other cardiac-related studies is
http://www.bidmc.harvard.edu/cmr/cmr-network.html

This URL provides links to other sites of interest. We encourage the use of the Internet to show current examples comparing CA with MRCA, successful and unsuccessful to help increase awareness on the problems and possible solutions that may be of interest to solve for the more technically oriented MR cardiac community.

References

1. Haase A, Matthaei D, Bartkowski E, Duhmke E, Leibfritz D (1989) Inversion recovery snapshot FLASH MR imaging. J Comput Assist Tomogr 13: 1036–1040
2. Matthaei D, Haase A, Henrich D, Duhmke E (1990) Cardiac and vascular imaging with an MR snapshot technique. Radiology 177: 527–532
3. Henrich D, Haase A, Matthaei D (1990) 3D-snapshot flash NMR imaging of the human heart. Magn Reson Imaging 8: 377–379
4. Edelman RR, Wallner B, Singer A, Atkinson DJ, Saini S (1990) Segmented turboFLASH: method for breath-hold MR imaging of the liver with flexible contrast. Radiology 177: 515–521
5. Atkinson DJ, Edelman RR (1991) Cineangiography of the heart in a single breath hold with a segmented turboFLASH sequence. Radiology 178: 357–360
6. Edelman RR, Manning WJ, Burnstein D, Paulin S (1991) Coronary arteries: breath-hold MR angiography. Radiology 181: 641–643
7. Meyer CH, Hu B, Nishimura DG, Macovski A (1992) Fast spiral coronary artery imaging. Magn Reson Med 28: 202–213
8. Simonetti OP, Finn JP, White RD, Laub G, Henry DA (1996) "Black blood" T2-weighted inversion-recovery MR imaging of the heart. Radiology 199: 49–57
9. McConnell MV, Goldfarb JW, Manning WJ, Edelman RR (1997) High-resolution black-blood coronary MR imaging using navigator gating [Abstract]. In: Book of Abstracts of the 5th Meeting of the International Society of Magnetic Resonance in Medicine (ISMRM) 2: 797
10. Wielopolski PA, Manning WJ, Edelman RR (1995) Breath-hold volumetric imaging of the heart using magnetization prepared 3D segmented echo planar imaging. J Magn Reson Imaging 4: 403–409
11. Jakob PM, Hillenbrand C, Sandstede J, Kenn W, Pabst T, Hahn D, Haase A (1999) MR-Cat scan: cardiac imaging with a new hybrid approach [Abstract]. In: Book of Abstracts of the 7th Meeting of the International Society of Magnetic Resonance in Medicine (ISMRM) 2: 1306
12. Paulin S, Schulthess GK von, Fossel E, Krayenbuenhl HP (1987) MR imaging of the aortic root and proximal coronary arteries. AJR 148: 665–670
13. Stehling MK, Holzknecht NG, Laub G, Bohm D, Smekal A von, Reiser M (1996) Single-shot T1- and T2-weighted magnetic resonance imaging of the heart with black blood: preliminary experience. MAGMA 4: 231–240
14. Edelman RR, Chien D, Kim D (1991) Fast selective black blood MR imaging. Radiology 181: 655–660

15. Duerinckx AJ (1999) Coronary MR angiography. Radiol Clin North Am 37: 273–318
16. Paschal CB, Haacke EM, Adler LP (1993) Three-dimensional MR imaging of the coronary arteries: preliminary clinical experience. J Magn Reson Imaging 3: 491–500
17. Li D, Paschal CB, Haacke EM, Adler LP (1993) Coronary arteries: three-dimensional MR imaging with fat saturation and magnetization transfer contrast. Radiology 187: 401–406
18. McConnell MV, Khasgiwala VC, Savord BJ, Chen MH, Chuang ML, Edelman RR, Manning WJ (1997) Comparison of respiratory suppression methods and navigator locations for MR coronary angiography. AJR 168: 1369–1375
19. Hofman MBM, Paschal CB, Li D, Haacke EM, Van Rossum AC, Sprenger M (1995) MRI of coronary arteries, 2D breathhold versus 3D respiratory-gated acquisition. J Comput Assist Tomogr 19: 56–62
20. Li D, Kaushikkar S, Haacke EM, Woodard PK, Dhawale P, Kroeker RM, Laub G, Kuginuki Y, Gutierrez FR (1996) Three-dimensional imaging of coronary arteries with retrospective respiratory gating. Radiology 201: 857–863
21. Oshinski JN, Hofland L, Mukundan S Jr, Dixon WT, Parks WJ, Pettigrew RI (1996) Two-dimensional coronary MR angiography without breath holding. Radiology 201: 737–743
22. Wang Y, Rossman PJ, Grimm RC, Riederer SJ, Ehman RL (1996) Navigator-echo-based real-time respiratory gating and triggering for reduction of respiration effects in three-dimensional coronary MR angiography. Radiology 198: 55–60
23. Thedens DR, Irarrazaval P, Sachs TS, Meyer CH, Nishimura DG (1999) Fast magnetic resonance coronary angiography with a three-dimensional stack of spirals trajectory. Magn Reson Med 41: 1170–1179
24. Irarrazabal P, Nishimura DG (1995) Fast three-dimensional magnetic resonance imaging. Magn Reson Med 33: 656–662
25. Stuber M, Botnar R, Danias PG, Sodickson DK, Kissinger KV, van Cauteren M, Becker J de, Manning WJ (1999) Double-oblique-breathing high resolution three-dimensional coronary magnetic resonance angiography. J Am Coll Cardiol 34: 524–531
26. Wielopolski PA, van Geuns RJ, de Feyter PJ, Oudkerk M (1998) Breath-hold coronary MR angiography with volume-targeted imaging. Radiology 209: 209–219
27. Slavin GS, Riederer SJ, Ehman RL (1998) Two-dimensional multishot echo-planar coronary MR angiography. Magn Reson Med 40: 883–889
28. Meyer CH, Hu BS, Yang PC, McConnell MV, Kerr AB, Brittain JH, Pauly JM, Macovski A, Nishimura D (1999) Spiral cardiac imaging with high-performance gradients [Abstract]. In: Book of Abstracts of the 7th Meeting of the International Society of Magnetic Resonance in Medicine (ISMRM) 1: 389
29. Wang Y, Christy PS, Korosec FR, Alley MT, Grist TM, Polzin JA, Mistretta CA (1995) Coronary MRI with a respiratory feedback monitor: the 2D imaging case. Magn Reson Med 33: 116–121
30. McConnell MV, Khasgiwala VC, Savord BJ, Chen MH, Chuang ML, Edelman RR, Manning WJ (1997) Prospective adaptive navigator correction for breath-hold MR coronary angiography. Magn Reson Med 37: 148–152
31. Danias PG, McConnell MV, Khasgiwala VC, Chuang ML, Edelman RR, Manning WJ (1997) Prospective navigator correction of image position for coronary MR angiography. Radiology 203: 733–736
32. Keegan J, Gatehouse PD, Taylor AM, Yang GZ, Jhooti P, Firmin DN (1999) Coronary artery imaging in a 0.5-Tesla scanner: implementation of real-time, navigator echo-controlled segmented k-space FLASH and interleaved-spiral sequences. Magn Reson Med 41: 392–399
33. Wang Y, Grimm RC, Rossman PJ, Debbins JP, Riederer SJ, Ehman RL (1995) 3D coronary MR angiography in multiple breath-holds using a respiratory feedback monitor. Magn Reson Med 34: 11–16
34. Taylor AM, Keegan J, Jhooti P, Gatehouse PD, Firmin DN, Pennell DJ (1999) Differences between normal subjects and patients with coronary artery disease for three different MR coronary angiography respiratory suppression techniques. J Magn Reson Imaging 9: 786–793
35. Brittain JH, Hu BS, Wright GA, Meyer CH, Macovski A, Nishimura DG (1995) Coronary angiography with magnetization-prepared T2 contrast. Magn Reson Med 33: 689–696
36. Botnar RM, Stuber M, Danias PG, Kissinger KV, Manning WJ (1999) Improved coronary artery definition with T2-weighted, free-breathing, three-dimensional coronary MRA. Circulation 22: 3139–3148
37. Brittain JH, Olcott EW, Szuba A, Gold GE, Wright GA, Irarrazaval P, Nishimura DG (1997) Three-dimensional flow-independent peripheral angiography. Magn Reson Med 38: 343–354
38. Manning WJ, Li W, Boyle NG, Edelman RR (1993) Fat-suppressed breath-hold magnetic resonance coronary angiography. Circulation 87: 94–104
39. Manning WJ, Li W, Edelman RR (1993) A preliminary report comparing magnetic resonance coronary angiography with conventional angiography. N Engl J Med 328: 828–832
40. Manning WJ, Li W, Wielopolski P, Gaa J, Kannam JP, Edelman RR (1994) Magnetic resonance coronary angiography: comparison with contrast angiography [Abstract]. In: Book of Abstracts of the 2nd Meeting of the Society of Magnetic Resonance (SMR)1: 368
41. Duerinckx AJ, Urman MK (1994) Two-dimensional coronary MR angiography: analysis of initial clinical results. Radiology 193: 731–738
42. Pennell DJ, Keegan J, Firmin DN, Gatehouse PD, Underwood SR, Longmore DB (1993) Magnetic resonance imaging of coronary arteries: technique and preliminary results. Br Heart J 70: 315–326
43. Post JC, Rossum AC van, Hofman MBM, De Cock CC, Valk J, Visser CA (1997) Clinical utility of two-dimensional breath-hold MR angiography in detecting coronary artery disease. Eur Heart J 18: 426–433
44. Yoshino H, Nitatori T, Kachi E, Yano K, Taniuchi M, Hachiya J, Ishikawa K (1997) Directed proximal magnetic resonance coronary angiography compared with conventional contrast coronary angiography. Am J Cardiol 80: 514–518
45. Post JC, van Rossum AC, Hofman MB, Valk J, Visser CA (1996) Three-dimensional respiratory-gated MR angiography of coronary arteries: comparison with conventional coronary angiography. AJR 166: 1399–1404
46. Müller MF, Fleisch M, Kroeker R, Chatterjee T, Meier B, Vock P (1997) Proximal coronary stenosis: three-dimensional MRI with fat saturation and navigator echo. J Magn Reson Imaging 7: 644–651
47. Huber A, Nikolaou K, Gonschior P, Knez A, Stehling M, Reiser M (1999) Navigator echo-based respiratory gating for three-dimensional MR coronary angiography: results from healthy volunteers and patients with proximal coronary artery stenoses. AJR 173: 95–101
48. Van Geuns RJM, de Bruin HG, Rensing BJWM, Wielopolski PA, Hulshoff MD, van Ooijen PMA, Oudkerk M, de Feyter PJ (1999) MRI of the coronary arteries: clinical results from three-dimensional evaluation of a respiratory gated technique. Heart 82: 515–519
49. Stehling MK, Balci C, Reiser M (1997) Navigator echo coronary MRA: controversial results [Abstract]. In: Book of Abstracts of the 5th Meeting of the International Society of Magnetic Resonance in Medicine (ISMRM) 2: 911
50. Lethimonnier F, Furber A, Morel O, Geslin P, Hoste PL, Tadei A, Jallet P, Caron-Poitreau C, Le Jeune JJ (1999) 3D MR coronary artery imaging with prospective real-time respiratory navigator: comparison with conventional coronary angiography [Abstract]. In: Book of Abstracts of the 7th Meeting of the International Society of Magnetic Resonance in Medicine (ISMRM) 2: 1257

51. Jhooti P, Keegan J, Gatehouse PD, Collins S, Rowe A, Taylor AM, Firmin DN (1999) 3D coronary artery imaging with phase reordering for improved scan efficiency. Magn Reson Med 41: 555–562
52. Yang GZ, Burger P, Gatehouse PD, Firmin DN (1999) Locally focused 3D coronary imaging using volume-selective RF excitation. Magn Reson Med 41: 171–178
53. Haacke EM, Patrick JL (1986) Reducing motion artifacts in two-dimensional Fourier transform imaging. Magn Reson Imaging 4: 359–376
54. Beck GM, Li D, Haacke EM, Noll TG, Kreitner KF, Voigtländer T, Schreiber WG, Thelen M (1999) Three-dimensional MR coronary angiography with a segmented echo-planar sequence and retrospective respiratory gating [Abstract]. In: Book of Abstracts of the 7th Meeting of the International Society of Magnetic Resonance in Medicine (ISMRM) 2: 1255
55. Botnar R, Stuber M, Kissinger KV, Danias PG, Manning WJ (1999) Free-breathing 3D coronary MRA with a fast TFE-EPI acquisition technique. In: Book of Abstracts of the 7th Meeting of the International Society of Magnetic Resonance in Medicine (ISMRM) 1: 233
56. Hardy CJ, McKinnon GC, Saranathan M (1999) High-resolution coronary artery imaging by adaptive averaging [Abstract]. In: Book of Abstracts of the 7th Meeting of the International Society of Magnetic Resonance in Medicine (ISMRM) 1: 231
57. van Geuns RJM, Wielopolski PA, de Bruin HG, van Ooijen PMA, Oudkerk M, de Feyter PJ (1998) VCATS: Volume coronary angiography using targeted scans, a new strategy in MR coronary angiography. Circulation 98:I-856
58. Wielopolski PA, Scharf JG, Edelman RR (1994) Multislice coronary angiography within a single breath-hold. J Magn Reson Imaging 4(P):80
59. Kessler W, Laub G, Achenbach S, Ropers D, Moshage W, Daniel WG (1999) Coronary arteries: MR angiography with fast contrast-enhanced three-dimensional breath-hold imaging: initial experience. Radiology 210: 566–572
60. Li D, Zheng J, Bae KT, Woodard PK, Haacke EM (1998) Contrast-enhanced magnetic resonance imaging of the coronary arteries. A review. Invest Radiol 33: 578–586
61. Regenfus M, Ropers D, Achenbach S, Kessler W, Moshage W, Laub G, Daniel WG (1999) Gadolinium-enhanced 3D breath-hold magnetic resonance angiography for detection of coronary artery stenosis in oblique projection angiograms. In: Book of Abstracts of the 7th Meeting of the International Society of Magnetic Resonance in Medicine (ISMRM) 2: 1262
62. Li D, Munger T, Zheng J, Kroeker R, Kim RJ, Simonetti OP, Haacke EM, Finn JP (1999) 3D breath-hold, firs-pass contrast-enhanced coronary artery imaging using MR fluoroscopic triggering, partial k-space acquisition, and inversion recovery. In: Book of Abstracts of the 7th Meeting of the International Society of Magnetic Resonance in Medicine (ISMRM) 2: 1260
63. Danias PG, Stuber M, Botnar RM, Kissinger KV, Chuang ML, Manning WJ (1998) Navigator assessment of breath-hold duration: impact of supplemental oxygen and hyperventilation. AJR 171: 395–397
64. Kimbiris D, Iskandrian AS, Segal BL, Bemis CE (1978) Anomalous aortic origin of coronary arteries. Circulation 58: 606–615
65. Chaitman BR, Lesperance J, Saltiel J, Bourassa MG (1976) Clinical angiographic, and hemodynamic findings in patients with anomalous origin of the coronary arteries. Circulation 53: 122–131
66. Levin DC, Fellows KE, Abrams HL (1978) Hemodynamically significant primary anomalies of the coronary arteries: angiographic aspects. Circulation 58: 25–34
67. McConnell MV, Ganz P, Selwyn AP, Li W, Edelman RR, Manning WJ (1995) Identification of anomalous coronary arteries and their anatomic course by magnetic resonance coronary angiography. Circulation 92: 3158–3162
68. Vliegen HW, Doornbos J, de Roos A, Jukema JW, Bekedam MA, van der Wall EE (1997) Value of fast gradient echo magnetic resonance angiography as an adjunct to coronary arteriography in detecting and confirming the course of clinically significant coronary artery anomalies. Am J Cardiol 79: 773–776
69. White RD, Caputo GR, Mark AS, Modin GW, Higgins CB (1987) Coronary artery bypass graft patency: non-invasive evaluation with MR imaging. Radiology 164: 681–686
70. Rubinstein RI, Askenase AD, Thickman D, Deldman MS, Agarwal JB, Helfant RH (1987) Magnetic resonance imaging to evaluate patency of aortocoronary bypass grafts. Circulation 76: 786–791
71. Gomes AS, Lois JF, Drinkwater DC, Corday SR (1987) Coronary artery bypass grafts: visualization with MR imaging. Radiology 162: 175–179
72. Jenkins JPR, Love HG, Foster CJ, Isherwood I, Rowlands DJ (1988) Detection of coronary artery bypass patency as assessed by magnetic resonance imaging. Br J Radiol 61: 2–4
73. Frija G, Schouman-Claeys E, Lacombe P, Bismuth V, Olivier JP (1989) A study of coronary artery bypass graft patecy using MR imaging. J Comput Assist Tomogr 13: 225–232
74. White RD, Pflugfelder PW, Lipton MJ, Higgins CB (1988) Coronary artery bypass grafts: evaluation of patency with cine MR imaging. AJR 150: 1271–1274
75. Galjee MA, van Rossum AC, Doesburg T, van Eenige MJ, Visser CA (1996) Value of magnetic resonance imaging in assessing patency and function of coronary artery bypass grafts. An angiographically controlled study. Circulation 93: 660–666
76. Aurigemma GP, Reichek N, Axel L, Schiebler M, Harris C, Kressel HY (1989) Noninvasive determination of coronary artery bypass graft patency by cine magnetic resonance imaging. Circulation 80: 1595–1602
77. Kessler W, Achenbach S, Moshage W, Zink D, Kroeker R, Nitz W, Laub G, Bachmann K (1997) Usefulness of respiratory gated magnetic resonance coronary angiography in assessing narrowings ≥ 50 % in diameter in native coronary arteries and in aortocoronary bypass conduits. Am J Cardiol 15: 989–993
78. Vrachliotis TG, Bis KG, Aliabadi D, Shetty AN, Safian R, Simonetti O (1997) Contrast-enhanced breath-hold MR angiography for evaluating patency of coronary artery bypass grafts. AJR 168: 1073–1080
79. Wintersperger BJ, Engelmann MG, Smekal A von, Knez A, Penzkofer HV, Hofling B, Laub G, Reiser MF (1998) Patency of coronary bypass grafts: assessment with breath-hold contrast-enhanced MR angiography: value of a non-electrocardiographically triggered technique. Radiology 208: 345–51
80. van Rossum AC, Galjee MA, Post JC, Visser CA (1997) A practical approach to MRI of coronary artery bypass graft patency and flow. Int J Cardiac Imaging 13: 199–204
81. Kalden P, Kreitner KF, Wittlinger T, Voigtlander T, Krummenauer F, Kestel J, Thelen MAJR (1999) Assessment of coronary artery bypass grafts: value of different breath-hold MR imaging techniques. AJR 172: 1359–1364
82. van Geuns RJ, Wielopolski PA, Rensing BJ, van Ooijen PM, Oudkerk M, de Feyter PJ (1999) Magnetic resonance imaging of the coronary arteries: anatomy of the coronary arteries and veins in three-dimensional imaging. Coronary Artery Dis 10: 261–267
83. Duerinckx AJ, Atkinson DP, Mintorovitvh J, Simonetti OP, Vrman MK (1996) Two-dimensional coronary MRA: limitations and artifacts. Eur Radiol 6: 312–325
84. Woodard PK, Li D, Haacke EM, Dhawale PJ, Kaushikkar S, Barzilai B, Braverman AC, Ludbrook PA, Weiss AN, Brown JJ, Mirowitz SA, Pilgram TK, Gutierrez FR (1998) Detection of coronary stenosis on source and projection images using three-dimensional MR angiography with retrospective respiratory gating: preliminary experience. AJR 170: 883–888
85. Edelman RR, Siewert B, Adamis M, Gaa J, Laub G, Wielopolski P (1994) Signal targeting with alternating radiofrequen-

cy (STAR) sequences: application to MR angiography. Magn Reson Med 31: 233–238
86. Wang SJ, Hu BS, Macovski A, Nishimura DG (1991) Coronary angiography using fast selective inversion recovery. Magn Reson Med 18: 417–423
87. Hennig J, Scheffler K, Laubenberger J, Strecker R (1997) Time-resolved projection angiography after bolus injection of contrast agent. Magn Reson Med 37: 341–345
88. Hardy CJ, Darrow RD, Pauly JM, Kerr AB, Dumoulin CL, Hu BS, Martin KM (1998) Interactive coronary MRI. Magn Reson Med 40: 105–111
89. Weber OM, Eggers H, Spiegel MA, Scheidegger MB, Boernert P, Boesiger P (1999) Interactive real-time MRI for the examination of left ventricular function [Abstract]. In: Book of Abstracts of the 7th Meeting of the International Society of Magnetic Resonance in Medicine (ISMRM) 2: 1299
90. Ridgway JP, Kassner A, Beacock DJ, Sivananthan UM (1999) Fast left ventricular volume measurement using a multiple-slice "real-time" acquisition: a pilot study [Abstract]. In: Book of Abstracts of the 7th Meeting of the International Society of Magnetic Resonance in Medicine (ISMRM) 1: 388
91. Bundy JM, Laub G, Kim R, Finn JP, Simonetti OP (1999) Real-time data acquisition for LV function [Abstract]. In: Book of Abstracts of the 7th Meeting of the International Society of Magnetic Resonance in Medicine (ISMRM) 1: 386
92. Sodickson DK, Stuber M, Botnar RM, Kissinger KV, Manning WJ (1999) SMASH real-time cardiac MR imaging at echocardiographic frame rates [Abstract]. In: Book of Abstracts of the 7th Meeting of the International Society of Magnetic Resonance in Medicine (ISMRM) 1: 387
93. Yang PC, Kerr AB, Liu AC, Liang DH, Hardy C, Meyer CH, Macovski A, Pauly JM, Hu BS (1998) New real-time interactive cardiac magnetic resonance imaging system complements echocardiography. J Am Coll Cardiol 32: 2049–2056
94. Grist TM, Korosec FR, Peters DC, Witte S, Walovitch RC, Dolan RP, Bridson WE, Yucel EK, Mistretta CA (1998) Steady-state and dynamic MR angiography with MS-325: initial experience in humans. Radiology 207: 539–544
95. Hofman MBM, Adzmli K, Brown J, Fisher S, Adams MD, Wickline SA, Lorenz CH (1997) Kinetics of a novel blood pool agent (MP-2269) with persistent high relaxivity for MR angiography [Abstract]. In: Book of Abstracts of the 5th Meeting of the International Society of Magnetic Resonance in Medicine (ISMRM) 1: 206
96. Alley MT, Napel S, Amano Y, Paik DS, Shifrin RY, Shimakawa A, Pelc NJ, Herfkens RJ (1999) Fast 3D cardiac cine MR imaging. J Magn Reson Imaging 9: 751–755
97. Rohl L, Ostergaard L, Simonsen CZ, Vestergaard-Poulsen P, Sorensen L, Bjornerud A, Saebo KB, Gyldensted C (1999) NC100150-enhanced 3D-SPGR MR angiography of the common carotid artery in a pig vascular stenosis model. Quantification of stenosis and dose optimization. Acta Radiol 40: 282–290
98. Duerk JL, Hurst GC (1994) Use of superparamagnetic contrast media to suppress signal from flowing spins: preliminary experience. J Magn Reson Imaging 4: 413–417
99. Weissleder R, Stark DD, Engelstad BL, Bacon BR, Compton CC, White DL, Jacobs P, Lewis J (1989) Superparamagnetic iron oxide: pharmacokinetics and toxicity. AJR 152: 167–173
100. Hamm B, Staks T, Taupitz M, Maibauer R, Speidel A, Huppertz A, Frenzel T, Lawaczeck R, Wolf KJ, Lange L (1994) Contrast-enhanced MR imaging of liver and spleen: first experience in humans with a new superparamagnetic iron oxide. J Magn Reson Imaging 4: 659–668
101. Johansson LO, Fischer SE, Lorenz CH (1999) Benefit of T1 reduction for magnetic resonance coronary angiography: a numerical simulation and phantom study. J Magn Reson Imaging 9: 552–556
102. Felblinger J, Lehmann C, Boesch C (1994) Electrocardiogram acquisition during MR examinations for patient monitoring and sequence triggering. Magn Reson Med 32: 523–529
103. Felblinger J, Debatin JF, Boesch C, Gruetter R, McKinnon GC (1995) Synchronization device for electrocardiography-gated echo-planar imaging. Radiology 197: 311–313
104. Vasanawala SS, Sachs TS, Brittain JH, Meyer CH, Nishimura DG (1999) Prospective MR signal-based cardiac triggering. Magn Reson Med 42: 82–86
105. Zimmermann-Paul GG, Quick HH, Vogt P, Schulthess GK von, Kling D, Debatin JF (1999) High-resolution intravascular magnetic resonance imaging: monitoring of plaque formation in heritable hyperlipidemic rabbits. Circulation 99: 1054–1061
106. Quick HH, Ladd ME, Zimmermann-Paul GG, Erhart P, Hofmann E, Schulthess GK von, Debatin JF (1999) Single-loop coil concepts for intravascular magnetic resonance imaging. Magn Reson Med 41: 751–758
107. Rivas PA, McConnell MV, Nayak K, Scott G, Meyer C, Pauly JM, Nishimura DG, Macovski A, Hu BS (1999) Real-time intravascular magnetic resonance receiver probe: In vivo observations in the rabbit aorta [Abstract]. In: Book of Abstracts of the 7th Meeting of the International Society of Magnetic Resonance in Medicine (ISMRM) 1: 82
108. Sodickson DK, Griswold MA, Jakob PM (1999) Smash imaging. Magn Reson Imaging Clin North Am 7: 237–254, vii–viii
109. Weiger M, Pruessmann KP, Gösele R, Leussler C, Röschmann P, Boesiger P (1999) Specific coil design for SENSE: a six-element cardiac array [Abstract]. In: Book of Abstracts of the 7th Meeting of the International Society of Magnetic Resonance in Medicine (ISMRM) 1: 162
110. Griswold MA, Jakob PM, Chen Q, Goldfarb JW, Manning WJ, Edelman RR, Sodickson DK (1999) Resolution enhancement in single-shot imaging using simultaneous acquisition of spatial harmonics. Magn Reson Med 41: 1236–1245
111. Sandstede JJ, Pabst T, Beer M, Geis N, Kenn W, Neubauer S, Hahn D (1999) Three-dimensional MR coronary angiography using the navigator technique compared with conventional coronary angiography. AJR 172: 135–139